DR 00418
DOE/ET/10815-88
(DE84008283)

Energy

FOSSIL

A ONE-DIMENSIONAL CODE TO PREDICT THE THERMAL BEHAVIOR OF THE UTSI MHD RADIANT FURNACE

Topical Report

By
Fred L. Galanga

March 1984

Work Performed Under Contract No. AC02-79ET10815

The University of Tennessee Space Institute
Energy Conversion Research and Development Programs
Tullahoma, Tennessee

Technical Information Center
Office of Scientific and Technical Information
United States Department of Energy

DISCLAIMER

DISCLAIMER

This report has been reproduced directly from the best available copy.

Available from the National Technical Information Service, U. S. Department of Commerce, Springfield, Virginia 22161.

Price: Printed Copy A03
Microfiche A01

Codes are used for pricing all publications. The code is determined by the number of pages in the publication. Information pertaining to the pricing codes can be found in the current issues of the following publications, which are generally available in most libraries: *Energy Research Abstracts (ERA); Government Reports Announcements* and Index (*GRA* and I); *Scientific and Technical Abstract Reports (STAR);* and publication NTIS-PR-360 available from NTIS at the above address.

DOE/ET/10815-88
(DE84008283)
Distribution Categories UC-90g and UC-93

A ONE-DIMENSIONAL CODE TO PREDICT THE THERMAL BEHAVIOR OF THE UTSI MHD RADIANT FURNACE

TOPICAL REPORT

Prepared By:

Fred L. Galanga

The University of Tennessee Space Institute
Energy Conversion Research and Development Programs
Tullahoma, Tennessee 37388

Final Released - March 1984

PREPARED FOR THE UNITED STATES
DEPARTMENT OF ENERGY

Under Contract No. DE-AC02-79ET10815

CONTENTS

FIGURES

NOMENCLATURE

A	heat transfer code
A_c	cross-sectional area
C	(with subscript) radiation correction factor
C	defined in equation 2.5.4
C_{f_x}	local skin friction coefficient
C_o	speed of electromagnetic wave propagation
C_p	specific heat
c_1	Planck's first constant
c_2	Planck's second constant
c_3	Constant in Wien's displacement law
dx	incremental axial length
e_b	blackbody hemispherical emissive power
E_g	gas emissive power
f_v	volume fraction of slag particles
g_c	gravitational constant
H	enthalpy
ΔH	enthalpy change
H_s	incident radiant flux density
h_{c_x}	local heat transfer coefficient
h_{eff}	effective heat transfer coefficient
k	thermal conductivity
k_e	extinction coefficient
L	length
$\dot{m}$	mass flow rate
n	index of refraction
Nu	Nusselt number

P	static gas system pressure
p	partial pressure of constituent
Pr	Prandtl number
Q	heat loss
$\dot{q}$	heat flux
Re	Reynolds number
r_e	electrical resistivity
St	Stanton number
T	temperature
t_{res}	residence time
u	velocity
W_s	leaving radiant flux density
x	defined in equation 2.5.3
α	absorptivity
δ	defined in equation 3.4.3
ε	emissivity
$\Delta\varepsilon$	emissivity correction for overlapping of emission bands
κ	effective soot emission parameter
λ	wavelength
μ	magnetic permeability
ρ	reflectivity
ρ_g	gas density
σ	Stefan-Boltzmann constant
τ_s	wall shear stress
ψ	Pentagamma function

Subscripts and Superscripts

b	refers to blackbody
c	refers to carbon dioxide
co	refers to carbon monoxide
conv	refers to convection
flame	refers to adiabatic flame condition
g	gas property
i,j	indices
o	vacuum condition
p	particle
r	refractory
rad	refers to radiation
rs	refractory/steel interface condition
s	gas-surface interface condition
st	steel
T	total condition
w	refers to water vapor
x	local axial condition

1.0 INTRODUCTION

The University of Tennessee Space Institute (UTSI) is presently engaged in testing and analysis of major components which simulate an open cycle MHD/steam power plant system. The facility, United States Department of Energy Coal Fired Flow Facility (CFFF), models important aspects of the system which are envisioned for commercial application (see Figure 1.1). Each component is designed to be compatible with the extremely high temperature plasma necessary for MHD power production. The system must efficiently recover heat while simultaneously controlling the levels of environmentally unacceptable gaseous emissions, notably NO_x and SO_x. Various test series have been and will be conducted to acquire engineering data which includes delineating the interaction between the various flow train components and assessing impact on the gas decomposition process.

Of critical importance in the overall research effort is the need for reliable analytical techniques to model the gas dynamic, thermal, and chemical kinetic behavior of the MHD combustion plasma throughout the MHD system. Such models are being actively pursued among the MHD and power plant community to provide a basis for characterizing the performance of the integrated MHD/steam power plant. Verification of these models against actual experimental results from an active facility is of utmost importance before they can be confidently used as tools for scaling to larger, commercial systems.

In this context, an analytical model of the thermal behavior of the radiant furnace components installed in the CFFF has been developed. Efforts have been primarily directed towards obtaining a representative global evaluation of the heat recovery of the major downstream components.

The gas dynamics throughout the radiant boiler are in the low Reynolds number regime and therefore are treated as a simple one-dimensional plug type flow. This simplification allows an explicit calculation of the local gas velocity and residence time via mass conservation. Chemical equilibrium of the plasma flow is assumed throughout the downstream system. Computations of the thermodynamic and transport properties of the gas are obtained from a combustion routine incorporated into the model. Calculation of the flow field properties is achieved explicitly by proceeding along the downstream flow train in a stepwise fashion and performing a thermodynamic balance at each step to account for the energy exchange between the fluid and its surroundings.

The primary mechanisms by which heat is transferred are via radiation and convection losses to the walls of the furnace. Coupled to these through the wall temperature boundary condition is a local calculation of the heat conduction through the composite wall structure of the various components. Calculations show that radiation from the combustion gas to the walls is the dominant mode of heat transfer. In the present model, the principal constituents participating in gas radiation are carbon dioxide, carbon monoxide, water vapor, and solid particles. Computation of the radiation properties of the working fluid as a whole is obtained by considering the contribution of each of the above species and correcting for overlapping emission bands. Both the total gas emissivity and its absorptivity are computed at each downstream computational station based upon

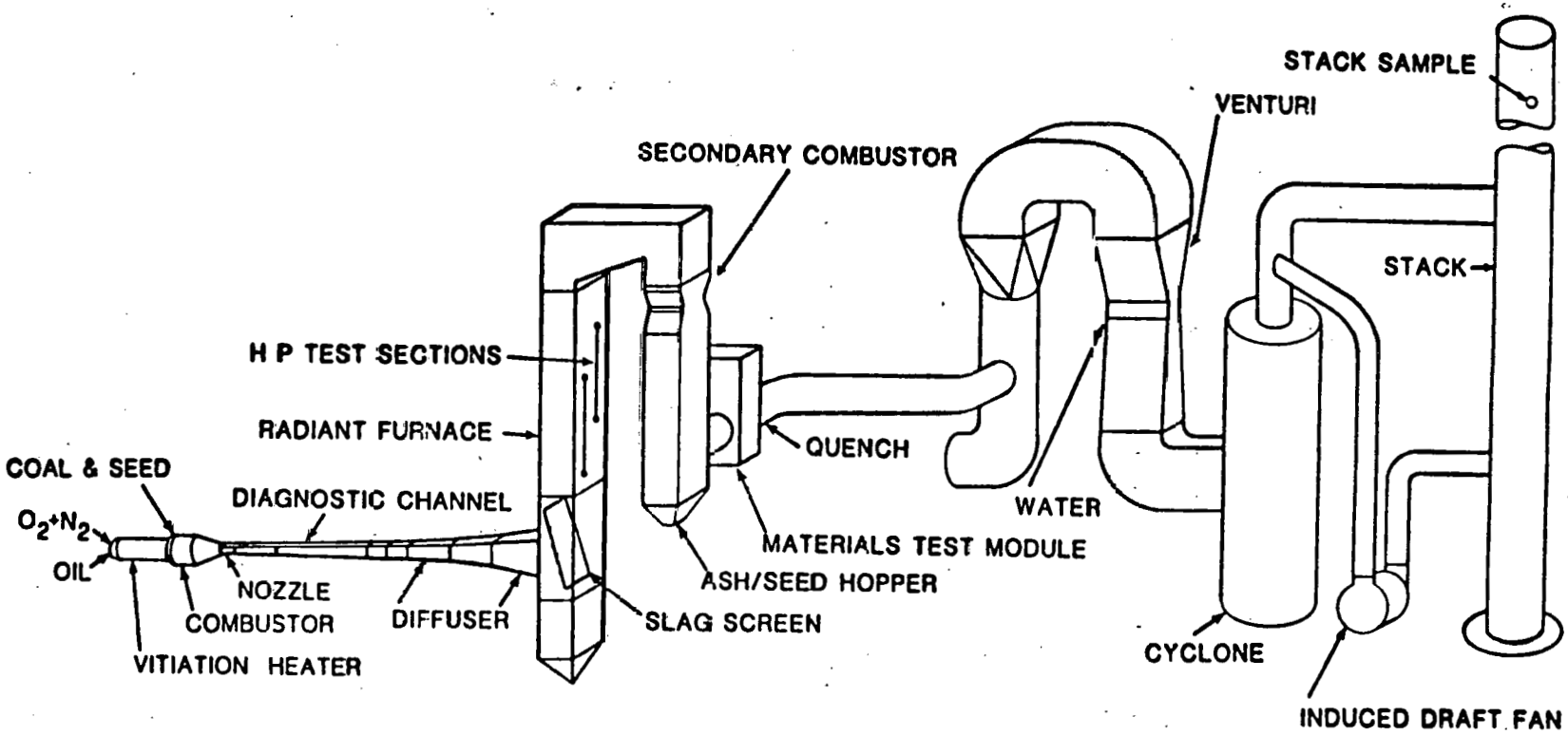

Figure 1.1 LMF1 Test Train Configuration

equilibrium chemistry of the gas and the local thermodynamic state. Radiation transport within a differential volume is treated as a single zone and gas-surface interchange is derived from first principles.

The purpose of this report is to describe the model and various routines which calculate the parameters necessary for solution. Section 2 is devoted to the radiation property calculations, while Section 3 describes the heat transfer model. Typical results are presented in Section 4.

2.0 EMISSIVITY AND ABSORPTIVITY CALCULATIONS

The primary mechanism by which heat is transferred in the radiant furnace is thermal radiation from water vapor, carbon dioxide, ash (i.e. slag particles) and carbon monoxide. Based on the work of Hottel and others,[1,2] and NASA SP-3080,[3] a computer code was developed to calculate the total emissivity of the gas. The total emissivity of the gas is determined by summing the individual total emissivities of each of the gaseous components and the slag particles and then making a correction for the overlapping of emission bands between the gases.

Similarly, the absorptivity is calculated, but here a correction must be included for the difference between the gas (which is absorbing) temperature and the wall (which is emitting) temperature. The corrections were obtained from Reference 4. A description of the emissivity and absorptivity calculation procedures follows.

2.1 CO_2 Emissivity and Absorptivity

Assume a hemispherical gas mass of radius L containing CO_2 at a partial pressure, p_c. Then consider the problem to be the evaluation of the radiant interchange between the gas at temperature, T_g, and a black element of surface at temperature, T_s, at the base of the hemisphere. The emission of the gas to the surface (per unit of surface area) is $\varepsilon_g T_g^4$, where ε_g is the ratio of radiation from gas to surface to the radiation from a blackbody at the same temperature, i.e. the emissivity. The emissivity of CO_2 depends on T_g, the product term p_c L, (i.e. the partial pressure times the beam length*) and the total pressure P_T. Radiation from CO_2 comes principally from bands at 2.64 to 2.84, 4.13 to 4.5, and 13 to 17 microns. Based on direct total measurements by Hottel and Manglesdorf[5] and Hottel and Smith[6] a smoothed plot of CO_2 emissivity, ε_c, at 1 atm total pressure is shown in Figure 2.1.1.

Thus the emissivity can be expressed (at one atmosphere total pressure) as

$$\varepsilon_c = \varepsilon_c (T_g, P_c L) . \qquad 2.1.1$$

Although the emissivity depends primarily on T_g and $p_c L$, pressure broadening does occur. Therefore, an empirical correction factor, C_c, for

*Beam length is the distance over which the radiative emission is taken.

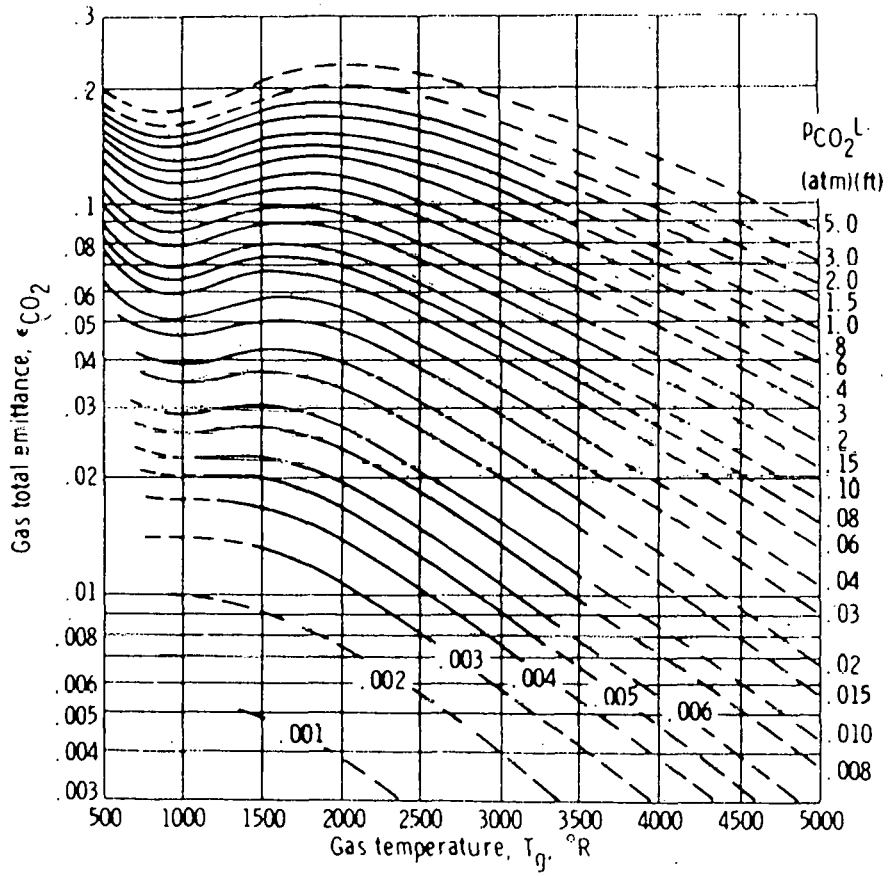

Figure 2.1.1 Emissivity of CO_2

total pressures other than one atmosphere can be introduced. Figure 2.1.2 is a plot of the correction factor versus total pressure. The value of ϵ_c when multiplied by C_c gives the correct value of emissivity when P_T is not one atmosphere.

The absorption by the gas from the surface is $\sigma T_s^4 \alpha_g$, where α_g is the gas absorptivity for blackbody radiation from a source at T_s. When $T_s = T_g$, $\alpha_g = \epsilon_g$; but as T_g increases above T_s, the absorptivity is affected by the temperature in two ways.

a) the molecular absorption coefficient increases slightly, but

b) the number of absorbing gas molecules in a fixed path length at a fixed partial pressure decreases.

Approximate empirical corrections can be made when α_g for CO_2 is evaluated at T_s and at $[p_c L\ (T_s/T_g)]$ instead of $p_c L$.

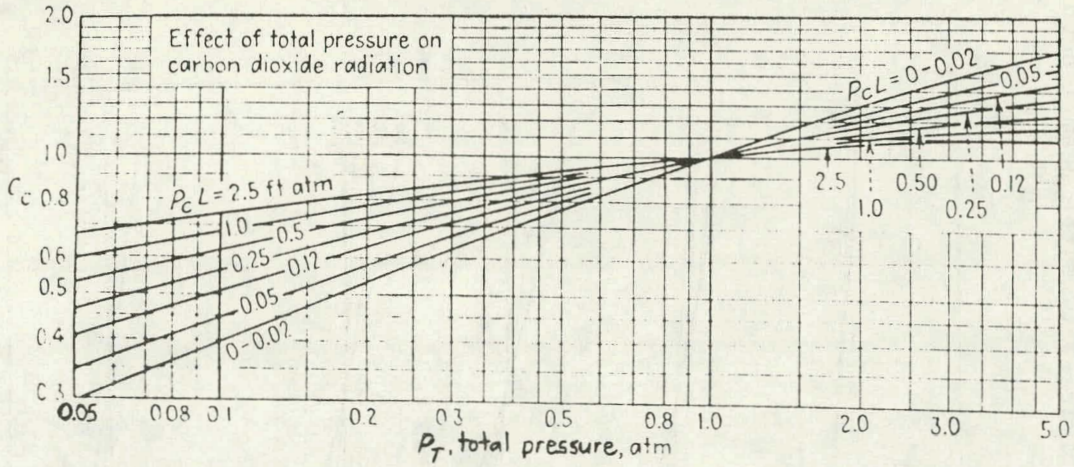

Figure 2.1.2 Pressure Broadening Correction Factor for CO_2 [Ref. 4]

In this case the absorptivity can be expressed as

$$\alpha_c = (T_g/T_s)^{0.65} \cdot \varepsilon_c[T_s,\ p_cL\ (T_s/T_g)] \qquad 2.1.2$$

In Figure 2.1.1, the total emissivity is plotted as a function of temperature and the product p_cL. The data were tabulated and a spline fit was used to obtain the emissivity at particular temperatures and pressure lengths. The computer subroutine first calculates the emissivity and then the absorptivity via use of equation 2.1.2. At this point in the program the total gas emissivity is set equal to the CO_2 emissivity, and then is adjusted as the contributions from the other reaction products are calculated.

2.2 H_2O Emissivity and Absorptivity

The emissivity of water vapor depends on T_g and p_wL, as in the case of CO_2, but also on the partial pressure p_w and total (i.e. gas system) pressure P. Radiation comes principally from bands at 2.55 to 2.84, 5.6 to 7.6 and 12 to 15 microns. At the first and third band there is an overlap with CO_2 emission which must be accounted for. (See Section 2.3.)

Total emissivity of water vapor is presented in Figure 2.2.1. Pressure broadening has a greater effect on H_2O emission than CO_2 emission. A pressure-broadening function, C_w, based on data from Hottel and Egbert[7,8] is presented in Figure 2.2.2. The value of ε_w from Figure 2.2.1 must be multiplied by the correction factor, C_w.

The absorptivity of H_2O may be obtained by evaluating ε_w at the wall surface temperature and by multiplying the result by $(T_g/T_s)^{0.45}$ or

$$\alpha_w(T_g,\ T_s,\ p_wL) = \varepsilon_w[T_w,\ p_wL\ (T_s/T_g)]\ (T_g/T_s)^{0.45} \qquad 2.2.1$$

The emissivity at this point can be expressed as

$$\varepsilon_g = C_c\ \varepsilon_c + C_w\ \varepsilon_w \qquad 2.2.2$$

Note: In these figures, ℓ is the beam length

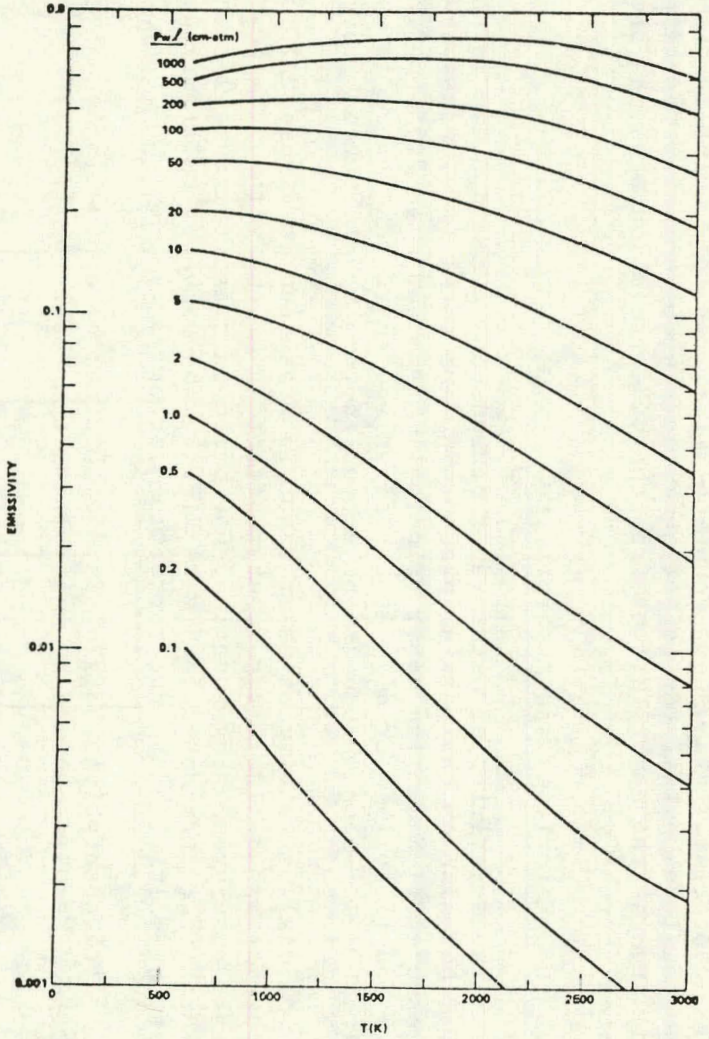

Figure 2.2.1 Emissivity of H_2O Vapor

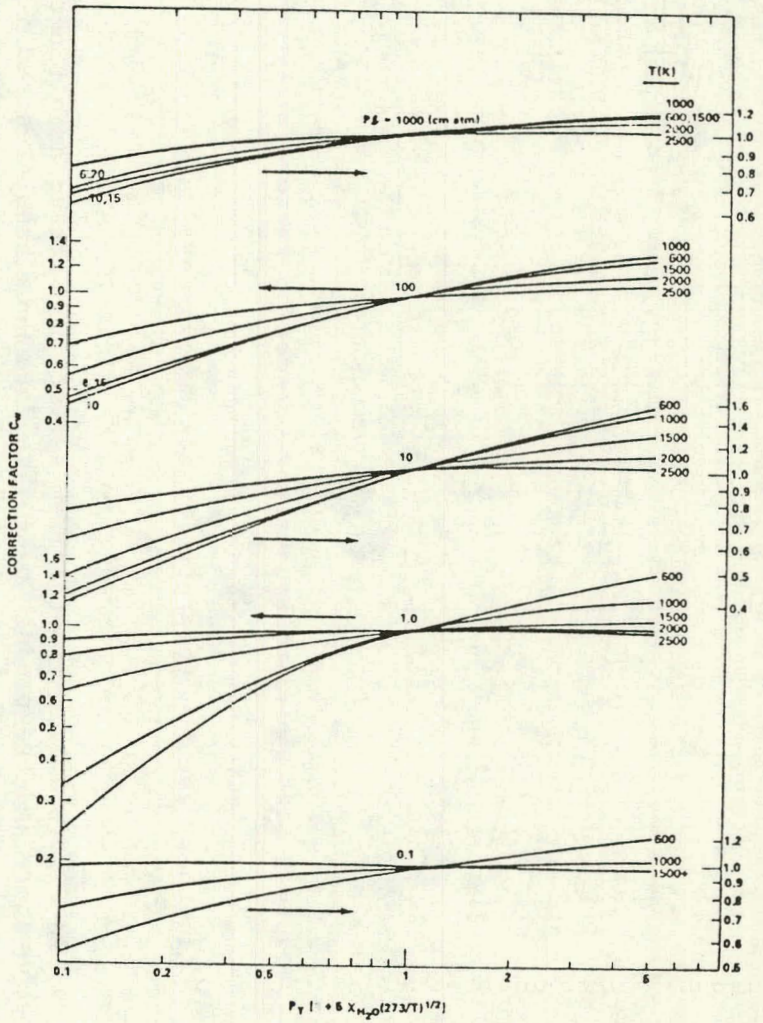

Figure 2.2.2 Correction Factor for H_2O Emissivity

[Ref. 3]

and the absorptivity as

$$\alpha_g = \alpha_c + \alpha_w \qquad 2.2.3$$

2.3 Correction for CO_2 - H_2O Interaction

When CO_2 and water vapor are present simultaneously the radiation is less than the sum of individual effects since the two gases are somewhat opaque to each other in the regions 2.7 and 15 microns. Therefore, a correction for this phenomenon can be applied such that the emissivity can be expressed as

$$\varepsilon_g = C_c\ \varepsilon_c + C_w\ \varepsilon_w - \Delta\varepsilon. \qquad 2.3.1$$

where $\Delta\varepsilon$ can be obtained from Figures 2.3.1.[4] The abscissa is the ratio of the partial pressure of water vapor to the sum of the partial pressures of CO_2 and H_2O. The correction data are plotted as a function of the sum of the partial pressures times the mean beam length in ft-atmospheres (i.e. $(p_c+p_w)L$). The corrections were determined at three gas temperatures, namely 400K, 811K and 1200K (260°F, 1000°F and 1700°F respectively). Figure 2.3.1.c is also valid for temperatures above 1200K (1700°F). Spline fits are again used to determine the emissivity and absorptivity at the particular gas and wall temperatures.

Analogously to the determination of $\Delta\varepsilon$, a correction $\Delta\alpha$ for absorptivity can be calculated, making the absorptivity for the case of CO_2 and H_2O

$$\alpha_g = \alpha_c + \alpha_w - \Delta\alpha \qquad 2.3.2$$

2.4 CO Emissivity and Absorptivity

Total radiation from carbon monoxide in nitrogen at one atmosphere has been measured by Ullrich[2], and the results are presented in Figure 2.4.1. Figure 2.4.1 is valid for gas temperatures up to 1275K (1840°F), and is shown for informational purposes only. The actual data used by the code was obtained from Ref. 3 which is valid to 3000K (4940°F) and is in tabular form. Spline fits of the data were programmed for calculation purposes. Hottel[4] recommends that the absorptivity be calculated from the following expression:

$$\alpha_{co}\ (T_g,\ T_s,\ p_{co}L) = (T_g/T_s)^{0.5}\ \ \varepsilon_{co}[T_s,\ p_{co}L\ (T_s/T_g)^{1.5}] \qquad 2.4.1$$

At this point, the gas emissivity can be expressed as

$$\varepsilon_g = C_c\ \varepsilon_c + C_w\ \varepsilon_w - \Delta\varepsilon + \varepsilon_{co} \qquad 2.4.2$$

and analogous to 2.4.2, the absorptivity is

$$\alpha_g = \alpha_c + \alpha_w - \Delta\alpha + \alpha_{co} \qquad 2.4.3$$

2.5 Particle Emission and Absorption

Many experimental investigations[9,10] have shown that the following expression closely correlates soot emission from luminous flames:

$$\varepsilon_p = 1 - e^{-\kappa L} \qquad 2.5.1$$

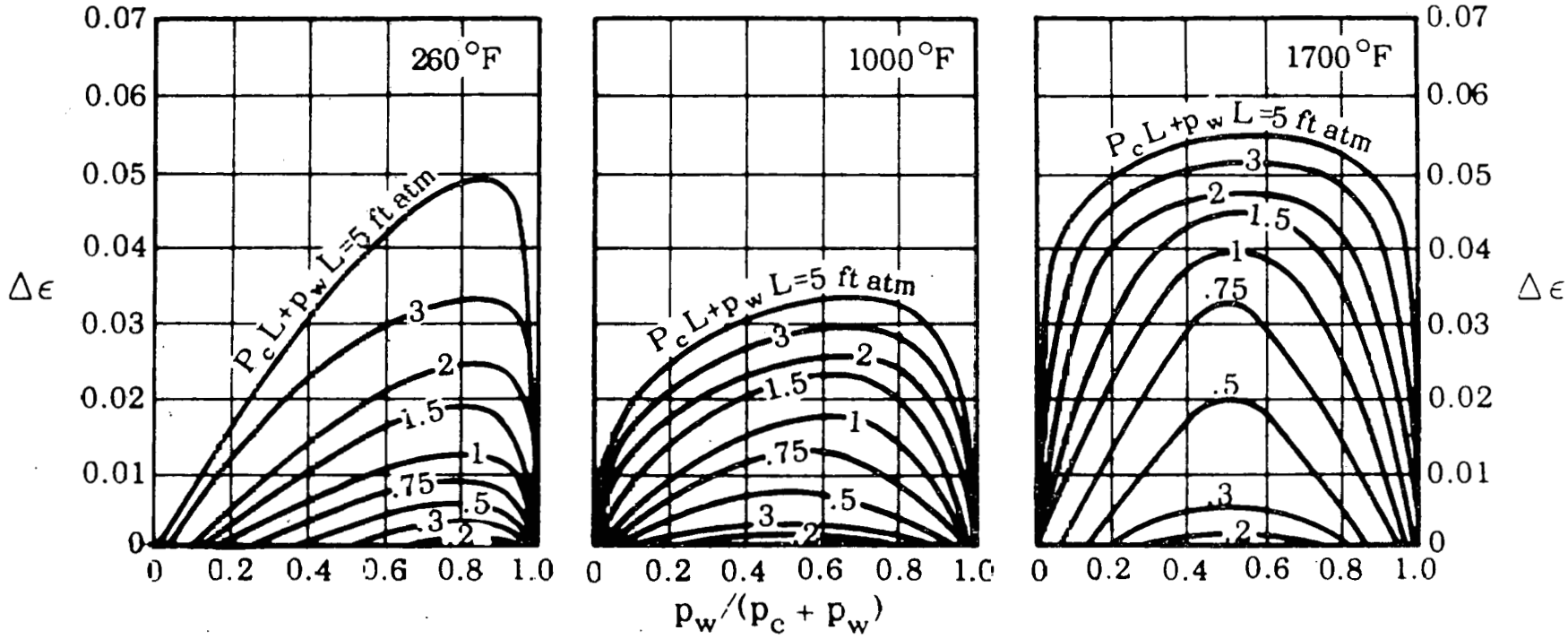

Figure 2.3.1 Correction Factors for CO_2-H_2O Interaction [Ref. 4]

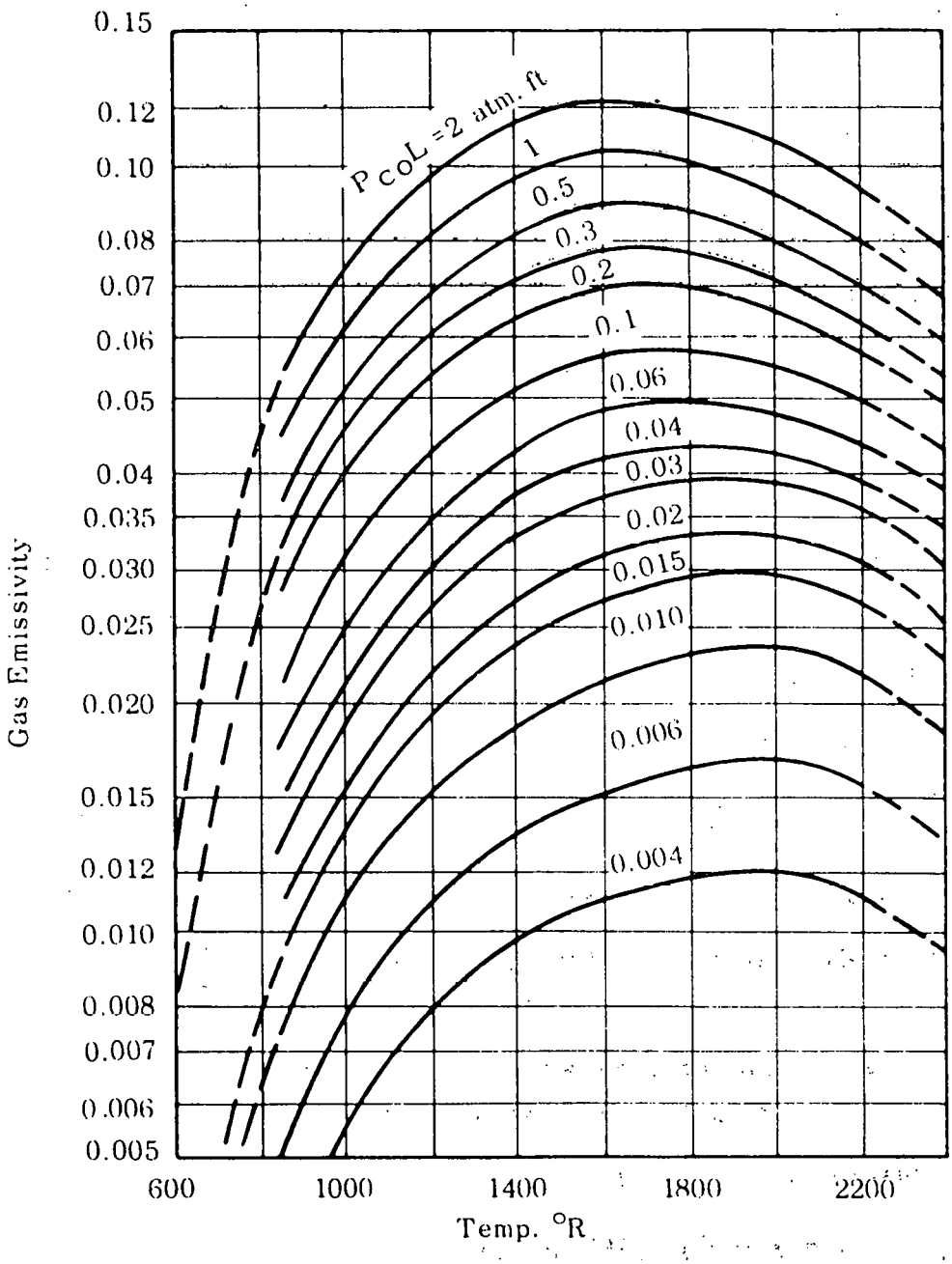

Figure 2.4.1 Emissivity of CO

where L is the beam length and κ is the effective soot emission parameter. This expression is a very good approximation to a closed form expression for soot emissivity based on a non-gray analysis

$$\varepsilon_p = 1 - \frac{15}{\pi^4} \psi^{3(1+x)} \qquad 2.5.2$$

where $x = \frac{CLT_g}{c_2}$ 2.5.3

and

$$C = 36\pi\, f_v \frac{nk_e}{[n^2-(nk_e)^2 + 2]^2 + (2nk_e)^2]} \qquad 2.5.4$$

where c_2 is Planck's second constant, f_v the volume fraction of soot particles and n and k_e are the index of refraction and extinction coefficient, respectively. If κ_e is given as

$$\kappa = 3.6 \frac{CT_g}{c2} \qquad 2.5.5$$

equation 2.5.1 can be expressed as

$$\varepsilon_p = 1 - e^{-3.6\ CT_gL/c2} \qquad \text{[Ref. 11]} \qquad 2.5.6$$

From the material properties of slag, the value of the index of refraction is set at 1.5. The extinction coefficient can be expressed as

$$k_e = \frac{\mu\lambda_o C_o}{4\pi r_e n} \qquad 2.5.7$$

where μ = magnetic permeability

C_o = speed of electromagnetic wave propagation in vacuum (2.9979×10^8 m/sec)

λ_o = wavelength in a vacuum

r_e = electrical resistivity, N m^2 sec/coulomb2

Assume

$\mu \approx \mu_o$ = magnetic permeability in a vacuum

$= 4\pi \times 10^{-7}$ N $sec^2/coulomb^2$

thus equation 2.5.7 becomes:

$$k_e \approx \frac{(4\pi \times 10^{-7})(2.9979 \times 10^8)\lambda_o}{4\pi\ r_e\ n}$$

which reduces to:

$$k_e \approx \frac{29.979\ \lambda_o}{r_e n} \approx \frac{30\lambda}{r_e n}$$

Based on the electrical properties of slag[12], the resistivity at a temperature of 2250K is approximately

$$r_e \approx 1 \text{ N sec}^2/\text{coulomb}^2$$

Therefore, equation 2.5.7.1 becomes:

$$k_e \approx \frac{30\lambda}{n} \qquad 2.5.8$$

The wavelength, λ, is determined at the point where the emissive power is maximum for a given temperature. From Planck's spectral distribution of blackbody hemispherical emissive power[13]

$$\frac{e_b}{T^5} = \frac{2\pi\, c_1}{(\lambda T)^5(\exp(c_2/\lambda T)-1)} \qquad 2.5.9$$

The maximum is found by differentiating equation 2.5.9 with respect to (λT) and setting the left hand side equal to zero, yielding

$$\lambda_{max}\, T = \frac{c_2}{5} \frac{1}{(1-\exp(-c_2/\lambda_{max}T))} \qquad 2.5.10$$

The solution is of the form

$$\lambda_{max}T = c_3 \qquad 2.5.11$$

which is a form of Wien's displacement law. The constant c_3 is 0.28978 cm-K. [Ref. 13] Based on the soot emission from a baked carbon electrode[14] at 2250K

$$\lambda = \frac{0.28978}{2250} = 1.288 \text{ X } 10^{-4} \text{ cm}$$

Therefore, using n = 1.5 from Reference 15, equation 2.5.8 yields

$$k_e \approx \frac{(30)\ (1.288 \text{ X } 10^{-4})}{1.5} \approx 2.58 \text{ x } 10^{-3}$$

Equation 2.5.6 can then be solved as a function of the gas temperature to determine the emissivity of the particles. In order to calculate the absorptivity, the wall temperature, T_s, is used in the equation in place of the gas temperature.

The total emissivity of the gas and particles can be finally expressed as:

$$\varepsilon_T = \varepsilon_g+\varepsilon_p-\varepsilon_g\varepsilon_p \qquad 2.5.12$$

where

$$\varepsilon_g = C_c\varepsilon_c + C_w\varepsilon_w - \Delta\varepsilon + \varepsilon_{co}$$

Similarly, the absorptivity can be expressed as

$$\alpha_T = \alpha_g + \alpha_p - \alpha_g\alpha_p \qquad 2.5.13$$

2.6 Method of Calculation

Radiation property calculations are incorporated in a series of subroutines to the main computer program. At each incremental step of the main program the emissivity and absorptivity are determined based on the initial wall temperature estimate. In order to permit these calculations to be made, the following parameters must be known a priori:

P - system total pressure (assumed constant)

P_C, P_{CO}, P_W - the partial pressures of the reaction products (CO_2, CO, and H_2O)

f_v - the volume fraction of slag particles

L - the beam length

The beam length is obtained from a subroutine which calculates the dimensions of the furnace. Beam length is taken as the average of the transverse dimensions in the cross sectional plane. Partial pressures are determined from the mole fractions of the individual gases. These are calculated over a range of temperatures in a combustion routine that has been incorporated into the model. An interpolation routine is used to obtain the mole fractions at the particular gas temperature of the incremental step. Volume fraction is calculated based on the mass and density of the slag and gas at the calculation point. Above the slag screen in the primary furnace, the radiation from the slag particles is neglected.

Once a wall (i.e. gas-refractory interface) temperature is assumed, an iteration process is used to determine the correct value based on the temperature projection through the composite wall. Each time a new wall temperature is assumed, a new total absorptivity is calculated. A new heat flux is determined and the process repeated until a solution is found. (See Section 3.7)

3.0 HEAT TRANSFER CODE

The heat transfer model developed treats the gas dynamics by assuming a one-dimensional plug type flow. In reality the flow is fully three-dimensional. In the radiant furnace, development of recirculation regions, flow stagnation on the slag screen, and vortex shedding off the slag tubes are but a few of the phenomena that occur. A one-dimensional model cannot account for these effects. However, in a global sense, an evaluation of the average conditions can be obtained and is very important for overall process evaluation studies and optimization.

Inputs to the model are the mass flow rates of the constituents, the stoichiometry of the reaction and the gas temperature at the diffuser exit plane. From these inputs, the combustion subroutine calculates the gas state properties over the temperature range expected. Transport properties, namely, viscosity and thermal conductivity, are determined from

results generated by a modified version of the NASA SP-273 combustion code[16] and curve fitted over this temperature range. A file is then generated and the properties at the calculated gas temperature are obtained by interpolation between the data base temperatures. This data base is valid to the axial location of secondary combustion, whereupon, a new combustion file is generated for the remainder of the temperature calculations to account for secondary combustion properties. In Figure 3.0.1 a simplified flow chart of the calculation procedure is presented.

The remainder of this section of the report is devoted to describing the method of code operation. Typical calculated results are compared to experimental data and presented in Section 4.

3.1 Area Determinations

As can be seen from Figures 3.1.1 through 3.1.3 the effluent gas passing through the radiant furnace negotiates a tortuous path as it passes through the slag screen and into the secondary furnace. Therefore, an "estimate" of the flow path, cross-sectional flow area, and surface area for heat transfer was determined. At various points along the flow train, the two transverse dimensions were tabulated for input into the model. A linear interpolation scheme was used to determine the dimensions at each incremental step. In addition, the beam length for radiation calculations was calculated as the average of the cross-sectional dimensions.

3.2 Axial Length Determinations

The approximate centerline of the flow area described in the previous section was chosen as the path length for the gas flow. The path length through the radiant furnace (Figure 3.1.1) was approximately five meters* (16.4 ft.), followed by a 7.3 m (24 ft) long constant area section, designated as the secondary furnace (not pictured). Path length through the top drum module, Figure 3.1.2, was calculated to be 6.1 m (20.1 ft) making a total length of 18.4 m (60.5 ft) to the secondary combustor inlet. The length of the secondary combustor and ash/seed hopper, Figure 3.1.3, (to the centerline of the crossover duct) is 6.1 m (20 ft). Therefore, the total path length of the system modeled is approximately 24.5 m (80.5 ft).

3.3 Gas Property Calculations

A combustion routine[17]** has been incorporated into the model for determination of parameters necessary for heat transfer calculations. This

* Subsequent to this work it has been experimentally determined that the average gas path length is approximately three feet less.

** This program was originally developed at Argonne National Laboratory. No date or author is available. Only state properties are calculated. Viscosity and thermal conductivity are calculated from curve fits to data[17].

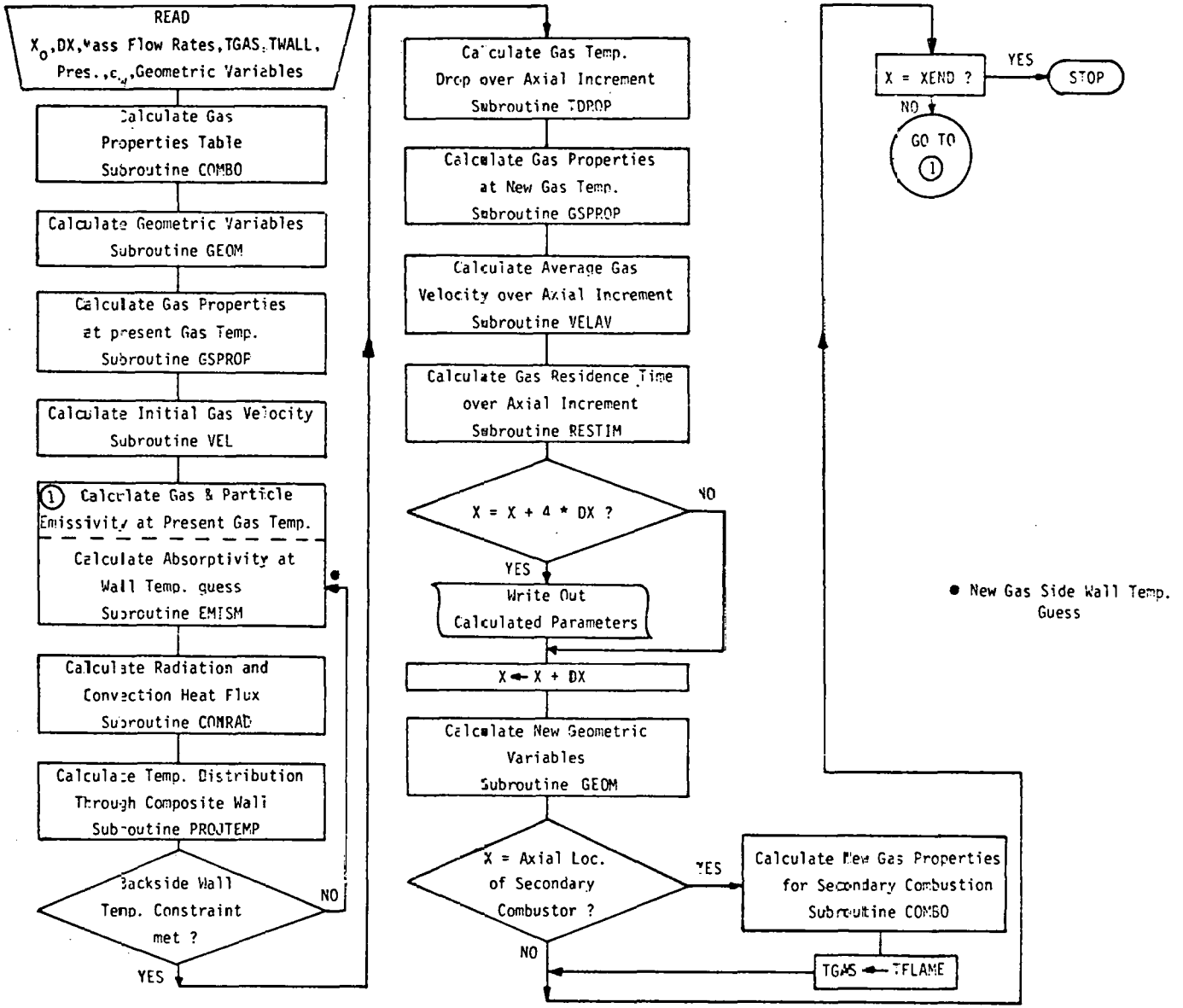

Figure 3.0.1 Simplified Flow Chart of Heat Transfer Code

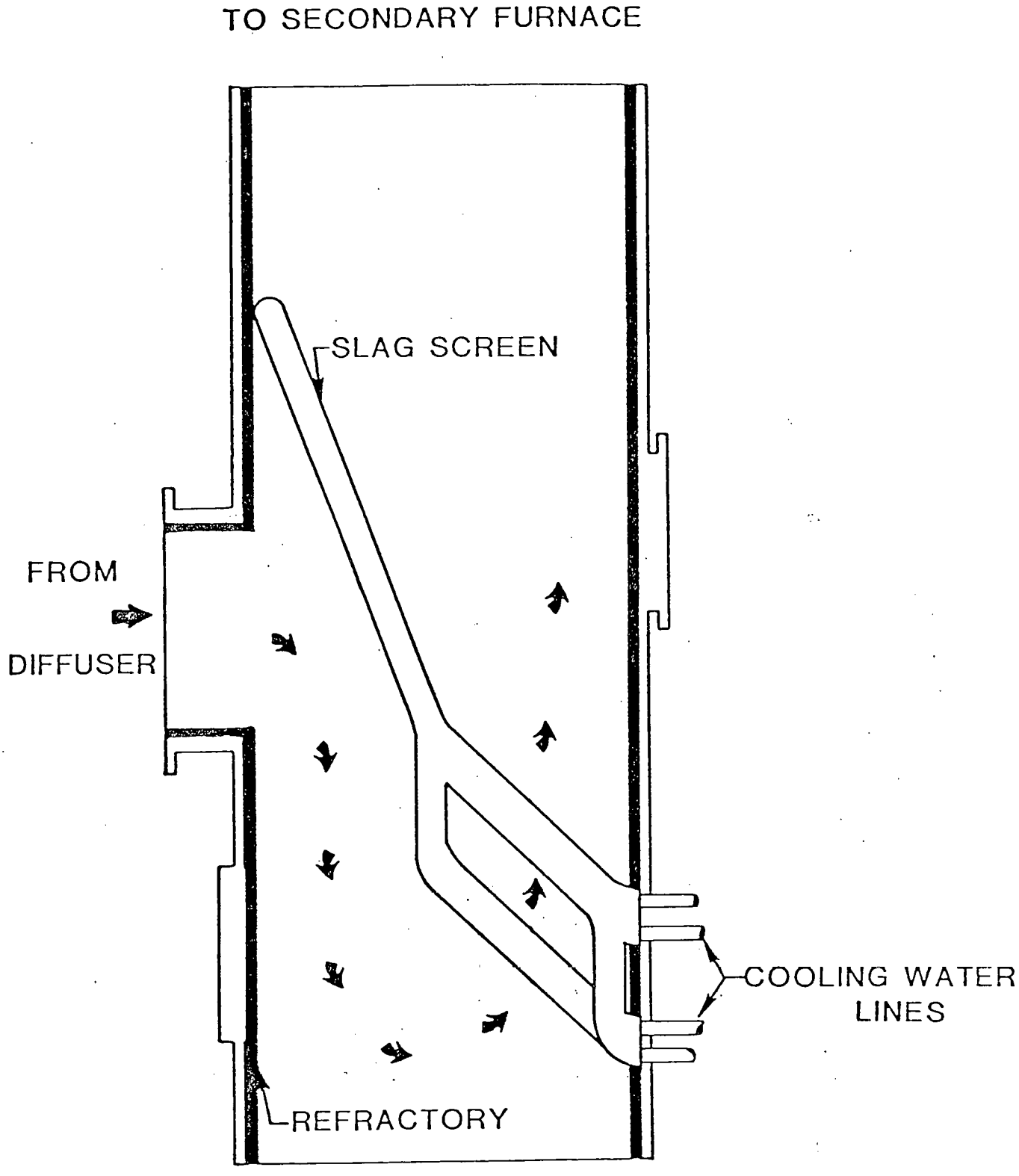

Figure 3.1.1 Primary Furnace Schematic

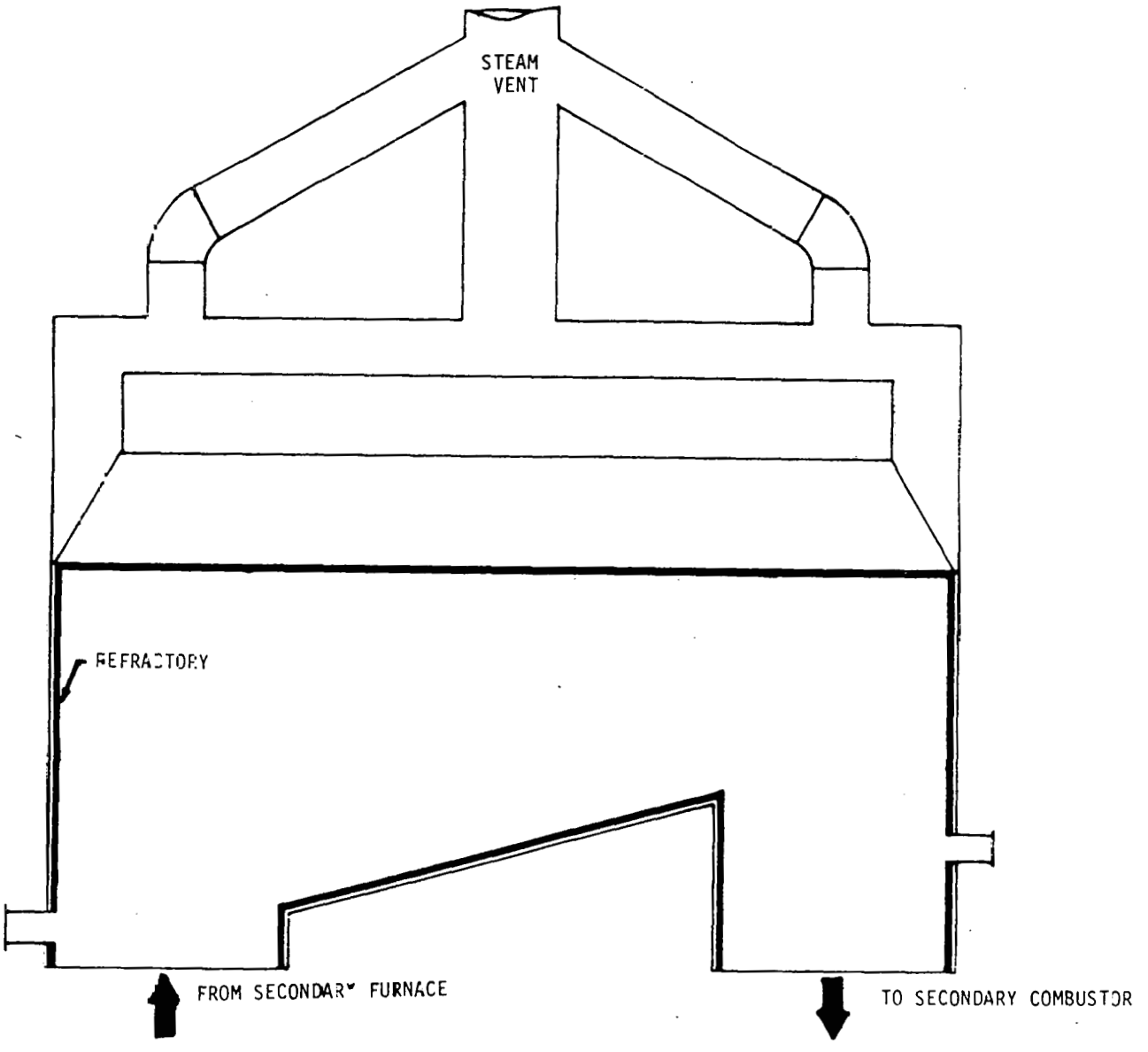

Figure 3.1.2 Top Drum Module Schematic

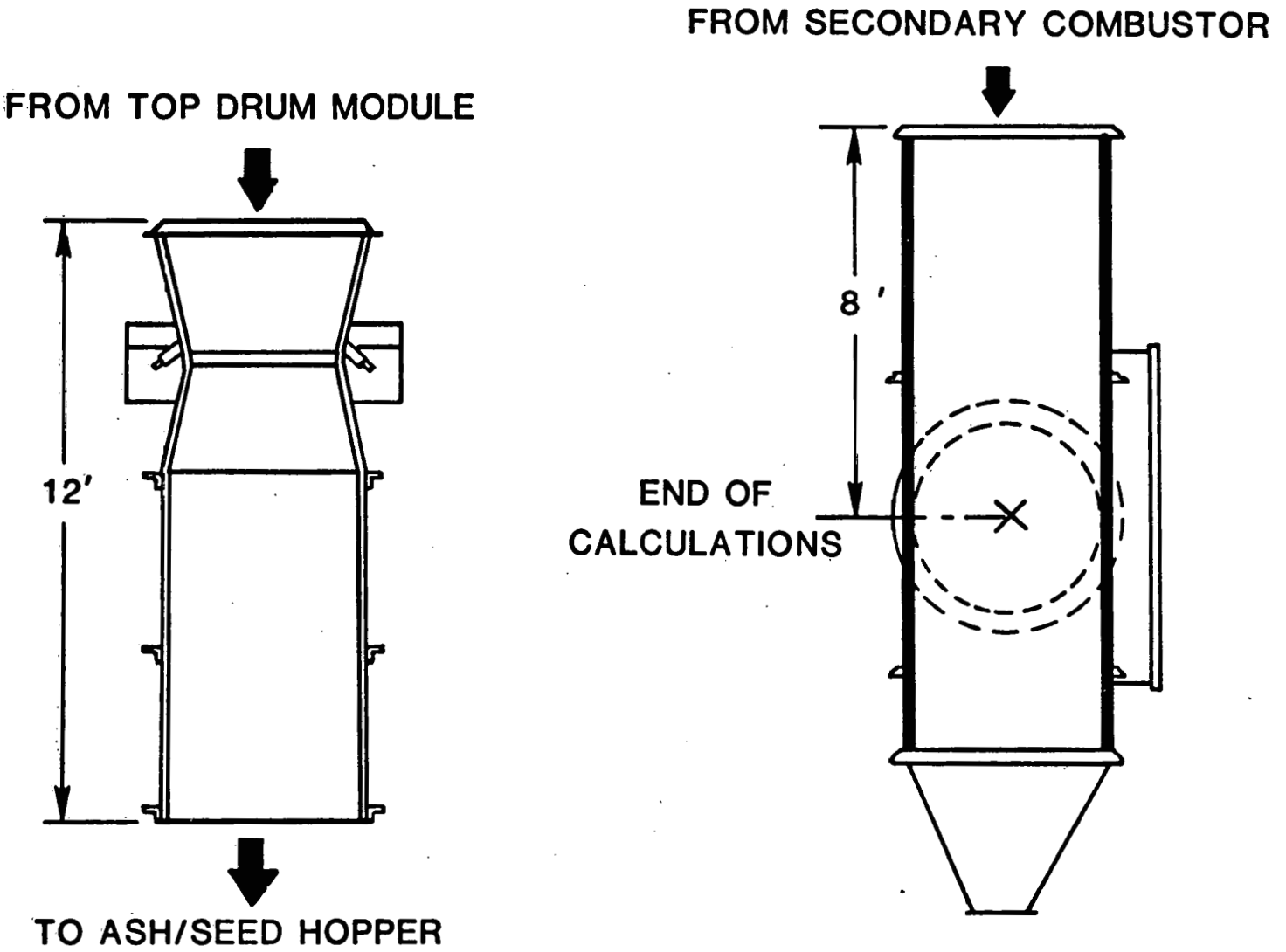

Figure 3.1.3 Secondary Combustor, Ash/Seed Hopper Schematic

routine accounts for contributions from thirteen species which sufficiently models the combustion process. The solutions obtained with this combustion routine are in very good agreement with results from reference 16. Figure 3.3.1 shows comparisons of various calculated parameters. The solid lines indicate the calculated values obtained from the adopted combustion routine, while the circular data points are values obtained from the modified NASA SP-273.

The thermodynamic states are obtained by minimization of Gibbs free energy. By characterizing the thermodynamic state by temperature and pressure, the Gibbs free energy is easily minimized since these are its natural variables.

The system is assumed to operate at constant pressure. Gas state and transport properties are tabulated over a temperature range of 1000K to 3100K which sufficiently bounds the temperatures encountered in the radiant furnace. A linear interpolation scheme determines the properties at a specified gas temperature. Properties determined from the calculation procedure are density, specific heat, viscosity, thermal conductivity, mole fractions (CO, CO_2 and H_2O), molecular weights and enthalpy.

3.4 Radiation and Convection Models

Since the gas is bounded by surfaces which are substantially uniform in temperature at each incremental step, the gas surface radiative interchange can be derived from first principles.[4] The radiation emitted by the gas can be expressed as

$$Q = A\varepsilon_T E_g \qquad 3.4.1$$

where A is the heat transfer surface area, ε_T is the total gas emissivity and

$$E_g = \sigma T_g^4 \qquad 3.4.2$$

σ being the Stefan-Boltzmann constant (5.67×10^{-12} w/cm^2 - K^4; 0.1713×10^{-8} BTU/ft^2 -hr-°R^4) and T_g the gas temperature.

A fraction α_s (equal to the surface emissivity ε_s for a gray surface) is absorbed at the surface, and a fraction ρ is reflected. (Note: by definition $(1-\rho) = \alpha = \varepsilon$). Likewise a fraction, δ, of the reflected radiation can be further absorbed and reflected at the walls. Summing the absorbed terms results in

$$Q = A\varepsilon_T E_g \varepsilon_s \left[1 + \rho\delta + (\rho\delta)^2 + (\rho\delta)^3 + \ldots\ldots\right] \qquad 3.4.3$$

The binomial series expansion in brackets reduces to

$$(1-\rho\delta)^{-1}$$

Therefore, Q can be expressed as

$$Q = \frac{A\varepsilon_T E_g \varepsilon_s}{(1-\rho\delta)} = \frac{A\,\varepsilon_T E_g \varepsilon_s}{1 - (1-\varepsilon_s)(1-\varepsilon_T)} \qquad 3.4.4$$

The net flux per unit surface area is $(W_s - H_s)$ where H_s is the incident radiant flux density and W_s is the leaving flux density. Incident flux density is composed of $\varepsilon_T E_g$ coming directly from the gas and $W_s (1-\alpha_T)$

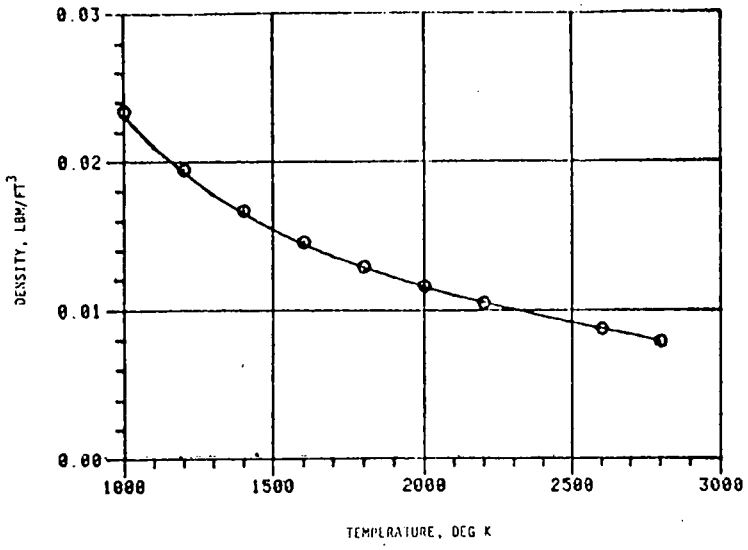

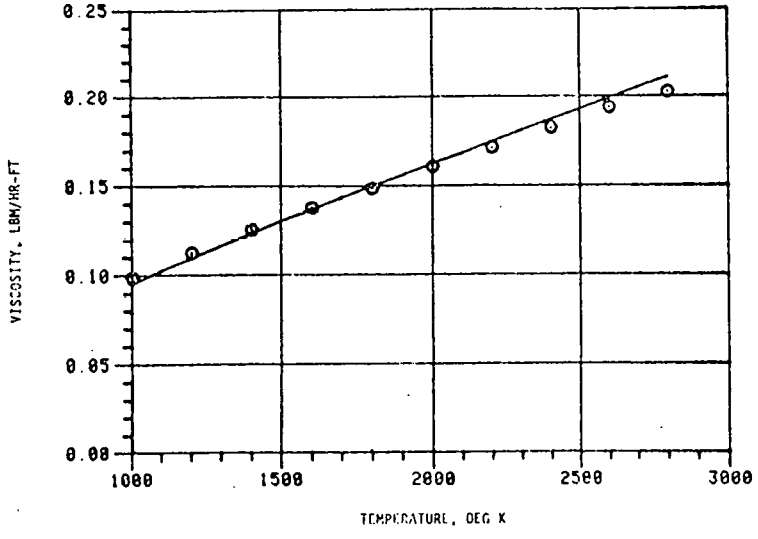

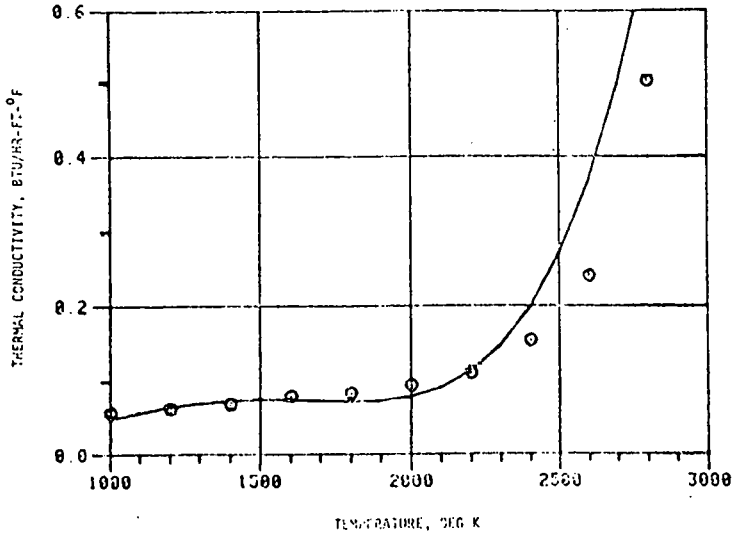

Figure 3.3.1 Comparison of Combustion Program Calculations

coming from opposite walls through the gas. Leaving flux density is composed of direct emission $\varepsilon_S E_S$ from the surface and reflected incident flux $H_S\ (1-\varepsilon_S)^4$.

Then

$$H_S = (1-\alpha_T)W_S+\varepsilon_T E_g \qquad 3.4.5$$

and

$$W_S = (1-\varepsilon_S)H_S + \varepsilon_S E_S \qquad 3.4.6$$

Solution of these two equations for H_S and W_S results in an expression for the net flux per unit area as

$$Q/A = \frac{\varepsilon_S \varepsilon_T E_g - \varepsilon_S \alpha_T E_S}{1 - (1-\alpha_T)(1-\varepsilon_S)}$$

or expressed in terms of temperature

$$Q/A = \frac{\varepsilon_S}{1 - (1-\alpha_T)(1-\varepsilon_S)}\ \sigma\ (\varepsilon_T\ T_g^4 - \alpha_T\ T_S^4) \qquad 3.4.7$$

Equation 3.4.7 was used as the basis for determination of the net radiative flux at each increment in the analytical solution. As described in Section 2.6, the gas emissivity is calculated at each step, while the absorptivity is computed each time a new wall temperature estimate is made. The wall emissivity, ε_S, was held constant at a value of 0.9 which is considered typical for boiler applications.

The convection portion of the heat flux model is based on the Reynolds analogy for turbulent flow over a flat plate. Since the dimensions of the radiant furnace are, in general, large, the four walls are treated as independent flat plates.

Strictly speaking, the Reynolds analogy is valid only for fluids with a Prandtl number of unity. The turbulent heat flux can be related to the turbulent shear stress as follows:

$$\frac{Q_S}{A} = g_c\ \tau_S C_p \frac{dT}{du} \qquad 3.4.8$$

Rearranging we obtain

$$dT = \frac{Q_S}{A\ \tau_S\ C_p\ g_c}\ du \qquad 3.4.9$$

Integrating between the limits u = 0 when T = T_S and u = u_g when T = T_g yields

$$\frac{Q_S}{A\ \tau_S\ C_p\ g_c}\ u_g = (T_g-T_S) \qquad 3.4.10$$

By definition

$$h_{cx} = \frac{Q_S}{A(T_g-T_S)} \text{ and } \tau_{Sx} = C_{fx}\ \frac{\rho u_g^2}{2g_c} \qquad 3.4.11a,b$$

Where h_{cx} is the local heat transfer coefficient, and C_{f_x} is the local skin friction coefficient. Equation 3.4.10 can be written as

$$\frac{h_{c_x}}{C_p \rho_g U_g} = \frac{Nu}{Re_x Pr} = \frac{C_{f_x}}{2} \qquad 3.4.12$$

Equation 3.4.12 can be modified for use with fluids in the Prandtl number range from 0.6 to 50 as follows[19]

$$\frac{Nu_x}{Re_x Pr} Pr^{2/3} = St_x Pr^{2/3} = \frac{C_{f_x}}{2} \qquad 3.4.13$$

where St_x is the local Stanton number.

For turbulent flow over a flat plate the empirical relation for the local skin friction coefficient is

$$C_{f_x} = 0.0576 \ (Re_x)^{-0.2} \qquad 3.4.14$$

Substituting 3.4.13 into 3.4.11 yields the local Nusselt number as

$$Nu_x = \frac{h_{cx} \ x}{k} = 0.0288 \ Pr^{1/3} \ Re_x^{4/5} \qquad 3.4.15$$

Substituting for h_{cx} from equation 3.4.11a and solving for $\frac{Q}{A}$ yields:

$$\frac{Q}{A} = 0.0288 \ \left(\frac{kg}{x}\right) Re^{4/5} Pr^{1/3} \ (T_g - T_s) \qquad 3.4.16$$

It should be noted here that the gas properties are evaluated at an average "film temperature", (i.e. $T_{film} = \frac{T_g + T_s}{2}$).

Combining equations 3.4.7 and 3.4.16 yields:

$$\dot{q}_T = \frac{Q}{A} = \frac{\varepsilon_s}{1-(1-\alpha_T)\ (1-\varepsilon_s)} \ \sigma \ (\varepsilon_T \ T_g^4 \ - \alpha_T \ T_s^4)$$
$$+ \ 0.0288 \ \frac{kg}{x} \ Re^{4/5} \ Pr^{1/3} \ (T_g - T_s) \qquad 3.4.17$$

Equation 3.4.17 was used as the basis for the heat transfer model in this study.

3.5 Slag Tube Calculations

An empirical correlation for heat transfer to a cylinder in crossflow was used as the convection model of the slag tubes. The recommended equations for Nusselt number are[20]:

At $Re = 1$ to 1×10^3

$$Nu = (0.43 + 0.50 \ Re^{0.5}) \ Pr^{0.38} \qquad 3.5.1$$

At $Re = 1 \times 10^3$ to 2×10^5

$$Nu = 0.25 \ Re^{0.6} \ Pr^{0.38} \qquad 3.5.2$$

As discussed in Section 3.4, the gas properties are evaluated at an average film temperature.

The slag screen is composed of a total of nine cylindrically shaped tubes, four tubes on the lower level and five tubes approximately 0.3m higher (Figure 3.1.1). It was assumed that the refractory temperature of the tubes was the same as the refractory wall temperature of the surrounding enclosure.

The radiation portion of the heat flux was calculated using equation 3.4.7 with the heat transfer area based on the total external surface area of each tube. Total heat loss contribution from the tubes was based on the number of tubes in each row and collectively lumped at two axial locations along with the contribution from the walled enclosure at these points.

3.6 Boundary Conditions

As shown in Figure 3.6.1, the wall of the radiant furnace is a composite structure comprised of refractory coated steel walls. Table 3.1 lists the refractories and approximate thicknesses used in the various components of the boiler. The steel wall thickness is 0.635 cm (0.25 inch). Beyond the steel wall is a 2.54 cm channel that is water-filled. This water continually boils off and is replenished with make-up water fed into the system near the top drum module.

The thermal conductivities of the refractories and steel are temperature-dependent. Polynomial curve fits of thermal conductivity were generated for the materials as a function of temperature. The functions are used at each incremental step in the model.

The only constraint imposed on the solution is that the water side steel wall temperature, T_{wH_2O} be fixed at 378 K (±1.7K) [220°F ±3°F]. From data obtained during LMFIA testing, this value appears quite reasonable. A solution at each incremental step is assumed if the projected temperature at this point matches the constraint. Otherwise a new refractory wall temperature was assumed, and an iterative technique used to obtain a solution. A more detailed explanation follows.

The boundary condition at the gas wall interface states that the total flux from the gas is equal to the product of the difference between the gas side wall temperature and the water side wall temperature multiplied by an effective heat transfer coefficient of the composite. Mathematically expressed

$$h_{eff}(T_s - T_{wH_2O}) = \dot{q}_{rad} + \dot{q}_{conv} = \dot{q}_T \qquad 3.6.1$$

The right hand side of this expression is equation 3.4.17 and the effective heat transfer coefficient is

$$h_{eff} = \frac{1}{\frac{L_r}{k_r} + \frac{L_{st}}{k_{st}}} \qquad 3.6.2$$

where L_r and L_{st} are the thicknesses of the refractory and steel, respectively.

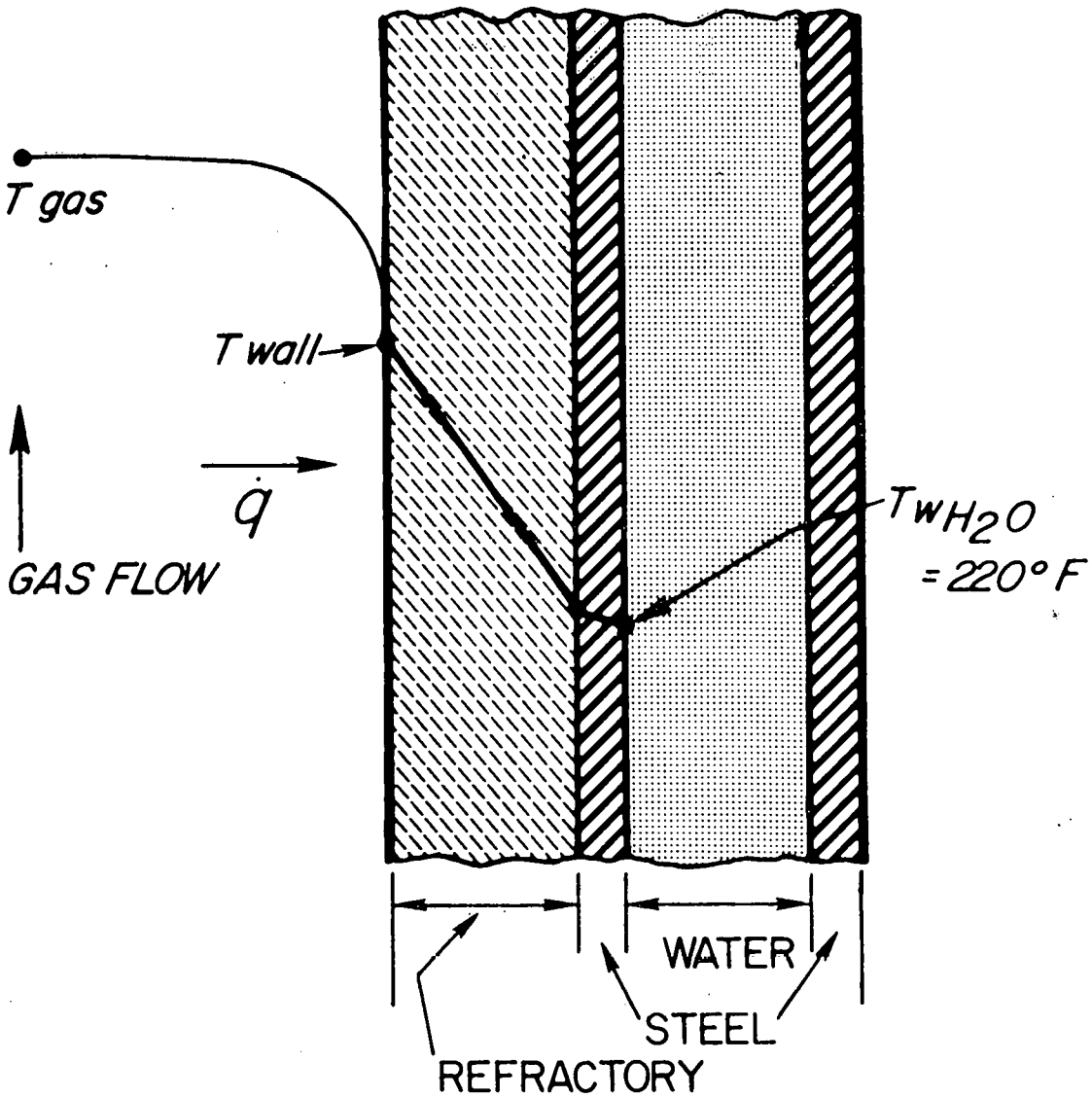

Figure 3.6.1 Schematic of Radiant Furnace Composite Wall

TABLE 3.1

COMPONENT	REFRACTORY	APPROX. THICKNESS (cm ; in)
Primary Furnace	Jade Pak 88P	2.54 ; 1.0
Secondary Furnace	Greencrete ARC	2.54 ; 1.0
Top Drum Module	Greencast 26L	7.62 ; 3.0
Secondary Combustor/ Ash Seed Hopper	Greencrete ARC	2.54 ; 1.0

Equation 3.6.1 can be rearranged and expressed as a fourth order polynomial in terms of the refractory wall temperature, T_s. This expression was solved at each step in the calculation to obtain a first approximation for the wall temperature.

3.7 Iterative Technique on Wall Temperature

The entrance gas temperature to the radiant furnace was provided from upstream thermo-fluid dynamic numerical solutions applied to the upstream[20]. At the initial step, an estimate of the wall temperature is input. Based on the gas temperature, the gas properties are calculated from the tabulated data using a linear interpolation scheme. Gas and particle emissivity and absorptivity is then calculated which permits a first estimate of the heat flux from equation 3.4.17. Based on the wall temperature, the refractory conductivity is determined and then the interface temperature between the refractory and steel, T_{rs}, is calculated from the following equation

$$T_{rs} = T_s - \frac{(\dot{q} \cdot L_r)}{k_r} \qquad 3.7.1$$

The thermal conductivity of the steel is then obtained and the water side steel temperature is calculated from the following equation

$$T_{w_{H_2O}} = T_{rs} - \frac{(\dot{q} \cdot L_{st})}{k_{st}} \qquad 3.7.2$$

If T_{wH_2O} does not match the constraint (± 3°F) then a new wall temperature is selected using a method of bisection. This process is repeated until the constraint is satisfied, whereupon a solution is assumed at the particular increment. The heat loss at this step is recalculated and a new gas temperature is determined for the next increment using the calorimetric balance

$$T_{gi+1} = T_{gi} - \frac{Q}{\dot{m}\, C_{pg}} \qquad 3.7.3$$

At each increment, the gas velocity is calculated from the continuity equation as

$$u_g = \frac{\dot{m}}{\rho_g\, A_c} \qquad 3.7.4$$

Finally the gas residence time and cumulative heat loss are summed at each step

$$t_{res} = \left[\sum_{j=1}^{i-1} (t_j)\right] + \left(\frac{dx}{u_g}\right)_i \qquad 3.7.5$$

and

$$Q_T = \left[\sum_{j=1}^{i-1} (Q_j)\right] + Q_i \qquad 3.7.6$$

3.8 Secondary Combustor Calculations

When the solution procedure reaches the axial location where secondary combustion occurs, the combustion subroutine is again called to recalculate gas properties with the addition of secondary air (79% N_2, 21% O_2). A new combustion file is generated for access by the main program. In addition, a determination of the secondary combustion flame temperature is made, as explained in the following discussion.

As part of the normal calculation scheme, the combustion adiabatic flame temperature is determined. The reference enthalpy level is at absolute zero temperature. Adiabatic flame enthalpy, H_{flame}, is calculated based on the heats of formation of the constituents. Before the gas has reached the secondary combustor, it has lost a substantial amount of energy. Therefore, an enthalpy change, ΔH, occurs and can be determined as the sum of all heat losses experienced by all the components upstream of the secondary combustor. This sum includes the experimentally determined total upstream heat loss, from the vitiation heater to the radiant furnace inlet, plus the calculated downstream loss, from radiant furnace inlet to the secondary combustor inlet. Therefore, the total change in specific enthalpy of the primary stream can be expressed as

$$\Delta H = [Q_{upstream} + Q_{downstream}]/\dot{m}_T \qquad 3.8.1$$

To find the enthalpy change occurring in the secondary combustion process, the flame enthalpy is added to the enthalpy loss, or

$$\Delta H_T = H_{flame} + \Delta H \qquad 3.8.2$$

Therefore, the flame temperature is determined by interpolation from the enthalpy table. At this point, the gas temperature is equated to the flame temperature at the enthalpy level.

4.0 RESULTS AND DISCUSSION

The output from the code has been compared to a number of experimentally measured test points to determine its accuracy. This section presents some typical calculated results compared to LMF1C test data obtained in the CFFF.

In Figures 4.1a and b, predicted gas temperature distributions from test LMF1C-5 are plotted as a function of the axial distance from the radiant furnace entrance to the centerline of the ash/seed hopper outlet. Conditions corresponding to the two test points considered are:

LMF1C-5 Test Cond.	$\dot{m}_T$ (Kg/s)	Primary N/O Ratio	Primary Stoichiometry	Thermal Input (MW)
Step 6	2.14	0.38	.82	17.4
Step 8	3.12	0.41	.92	23.9

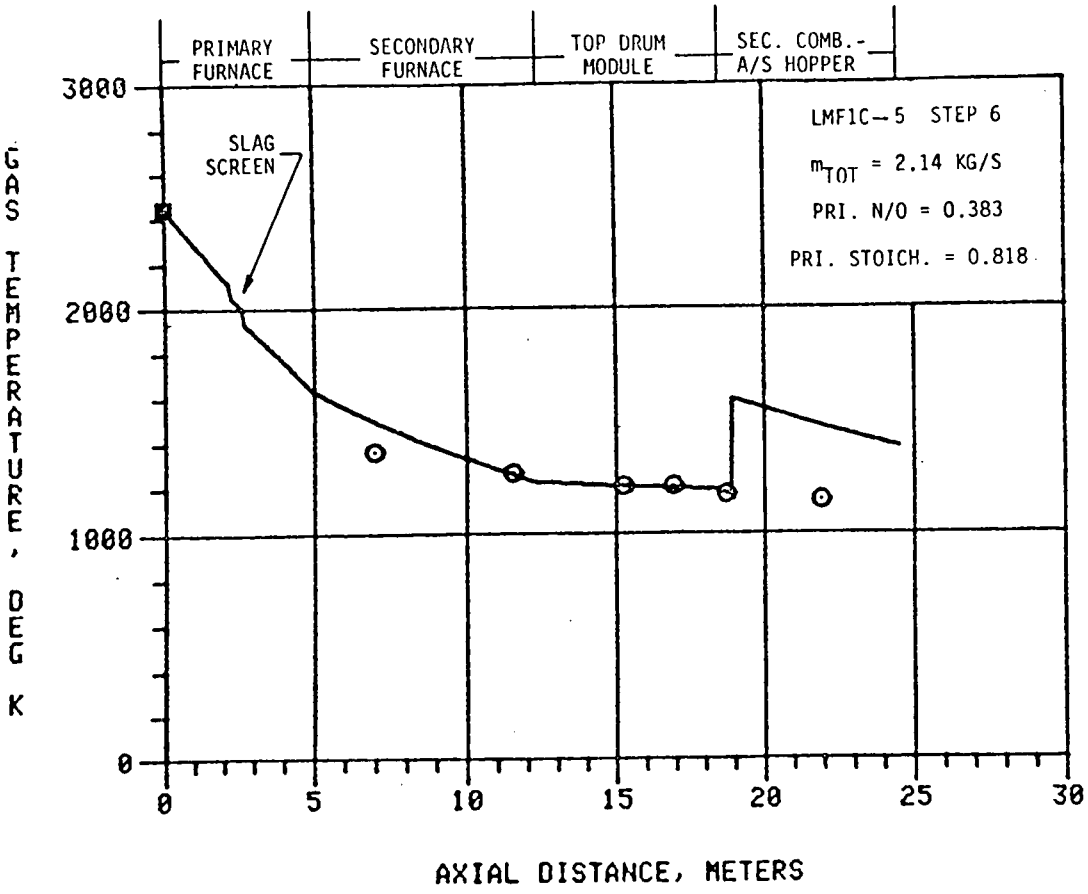

Figure 4.1a Gas Temperature Distribution, Test LMF1C-5, Step 6

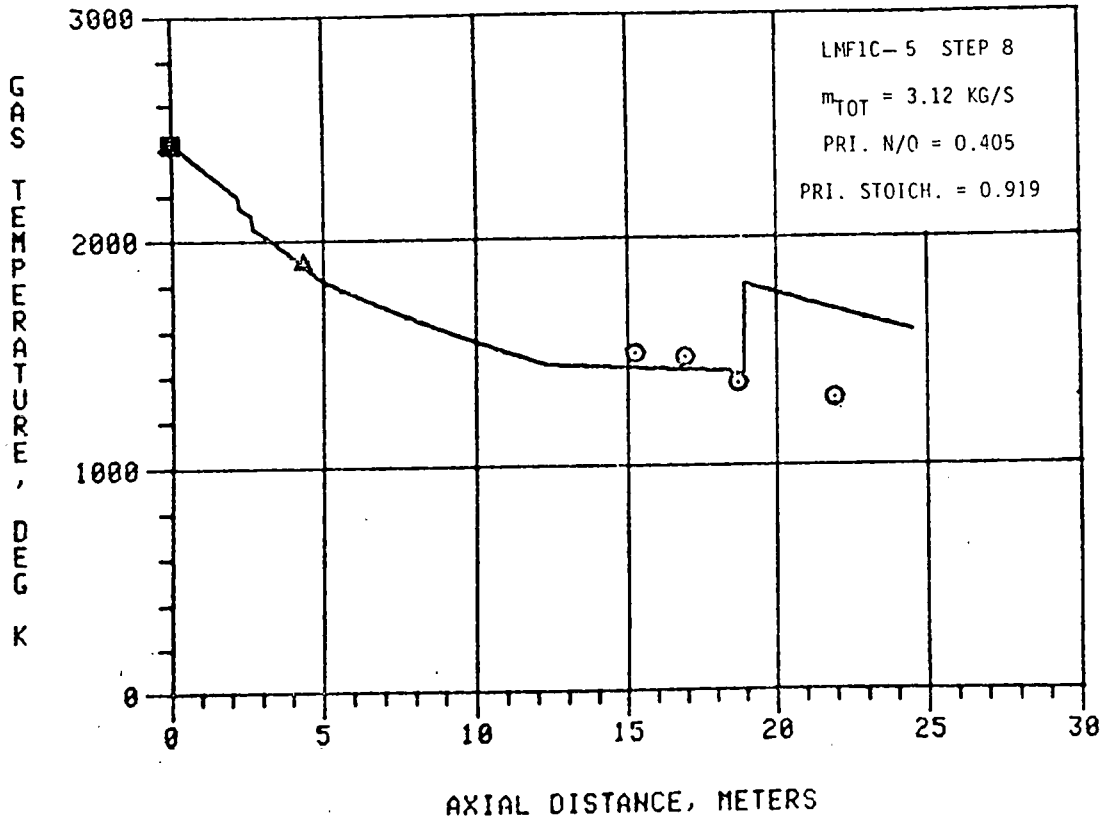

Figure 4.1b Gas Temperature Distribution, Test LMF1C-5, Step 8

During Step 6, six thermocouples in alumina protection tubes were operational. The data shown in Figure 4.1a represent two minute time averaged gas temperatures. Agreement is seen to be quite good up to secondary combustion. The thermocouple reading downstream of the secondary combustor deviates markedly from prediction. Investigation revealed that this particular thermocouple was not properly referenced, which could lead to a major source of measured temperature error. Other possibilities include the following:

a) Error produced by thermal radiation from the probe. Since the computed wall temperature is well below the gas temperature, the probe reading should be corrected for the radiation loss due to this temperature difference. This correction would increase the experimental temperature value. Methods of approximating this error are being investigated.

b) Enthalpy change of the gas. As demonstrated in Section 3.8, the flame temperature calculation is dependent on the amount of energy the gas has lost prior to the secondary combustor. However, the additional loss in the secondary combustor itself is not taken into account. Since the combustor is not independently cooled, an experimental value cannot be obtained. Any additional loss results in an additional enthalpy change which in effect lowers the flame temperature further. This effect is also being investigated.

c) Penetration depth of the probe. Subsequent to this analysis experimental gas temperature profiles have been obtained. The data indicate that a thermal boundary layer of significant thickness exists. Therefore, the probe reading may not be truly representative of the average gas temperature.

At Step 8, only four thermocouples (indicated by circular data points) were functioning, two in the top drum module and two in the secondary combustor. In addition to these measurements, two optical temperature measurements were obtained. The first measurement was obtained by a potassium line reversal system (indicated by the square symbol) located at the diffuser exit. This measurement confirms that the initial gas temperature input to the code, which was obtained from an analysis of the upstream heat transfer, is correct.

The second optical measurement (indicated by the triangular symbol) was obtained using a luminosity temperature system located immediately downstream of the slag screen. This system provides a relative temperature rather than an absolute measurement. Based on the emissivity of the gas measured by the line reversal system, an absolute value of the gas temperature was calculated. Agreement again is shown to be very good.

Other points of interest indicated in Figure 4.1b include:

a) At the slag screen location, two step-decreases in temperature are indicated. Physically, a step decrease in the gas temperature does not occur. In this region of the calculation procedure, the energy extracted from the gas by the slag tubes and the furnace

walls is lumped at two axial locations corresponding to the centerlines of the two sets of slag tubes. This basically annunciates the effect of the additional amount of energy that is removed from the gas as it passes over the screen.

b) The effect of the various refractories that coat the walls of the components of the radiant furnace is pronounced. This phenomenon is reflected by the changing slope of the gas temperature curve at three specific axial locations. Refractory interface points are located at 5, 12.3 and 18.4 M downstream of the furnace inlet section.

In the top drum module (TDM) the refractory used (Greencast 26L, a calcium-aluminate bonded insulating castable) has a very low thermal conductivity (~0.26 w/m^2-K, 0.15 Btu/hr-ft-°F). This is demonstrated by the small temperature decrease in this component indicating that very little heat is transferred to this component. In contrast, the refractory used in the radiant furnace (Jade Pak 88P) has a thermal conductivity which is an order of magnitude greater. Therefore, the energy removed from the gas stream in this region is also much greater.

In Figure 4.2a the cumulative heat loss corresponding to test LMF1C-5, Step 8 is presented. For this particular step, the predicted heat loss is approximately 6 MW which represents 25% of the total thermal input. An experimental value of heat loss is difficult to obtain. The major portion of the radiant furnace is cooled by water located in a jacket which surrounds the walls of the furnace. The water continually boils off, releasing steam to the atmosphere through vents located atop the top drum module. A water level indicator in the TDM senses a low limit and makeup water is fed into this component on an intermittent basis. In order to determine the amount of water that is fed into the system, a time average over a long interval is needed. During this time period, gas flow conditions are changed in order to achieve the objectives of the test matrix. Therefore, this bulk heat loss is a "best estimate" from available instrumentation. The bulk heat loss coupled with the losses measured from the independently cooled slag screen and various access ports and doors provides a total loss estimate. For this particular case, the experimental value obtained was about 7% lower than the predicted value.

The local heat flux distribution for Step 8 is shown in Figure 4.2b. As can be seen, the heat flux in the top drum module is nearly constant and minimal (< 1 W/cm^2). Figures 4.3a and b present the average gas velocity and cumulative residence time for this step. Average velocity is calculated from continuity and is a function of the gas density and flow cross-sectional area. The effect of the constrictions caused by the slag tubes is reflected in the two velocity spikes in this region. Thereafter the flow area expands to a constant 1.49 m^2 (16 ft^2) square cross-section in the secondary furnace. Here a gradual velocity decrease occurs as energy is removed and the density increases. The flow area again expands in the initial part of the TDM and a further velocity decrease is observed. The last peak occurs at the throat of the secondary combustor. Flow velocity exiting the ash/seed hopper is approximately 12 M/S (39.4 ft/sec).

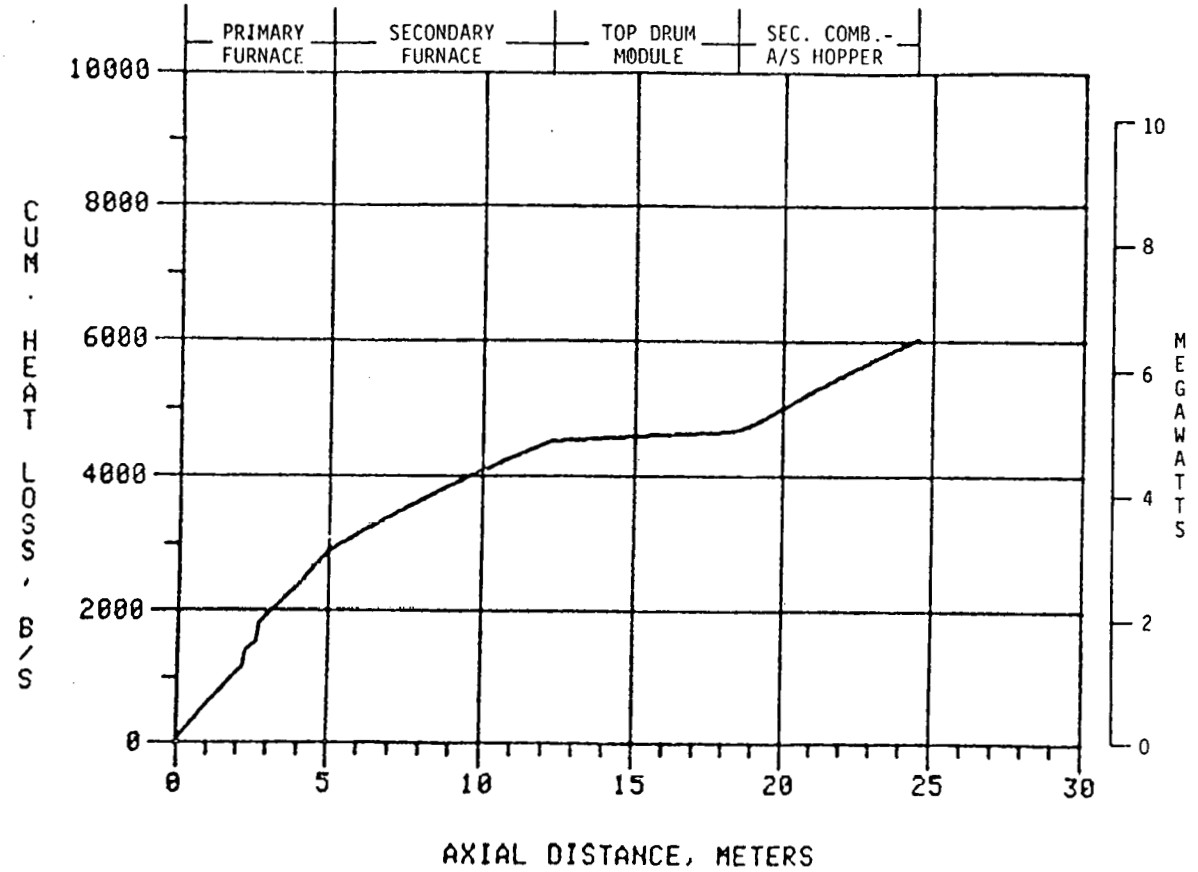

Figure 4.2a Cumulative Heat Loss Distribution, Test LMF1C-5, Step 8

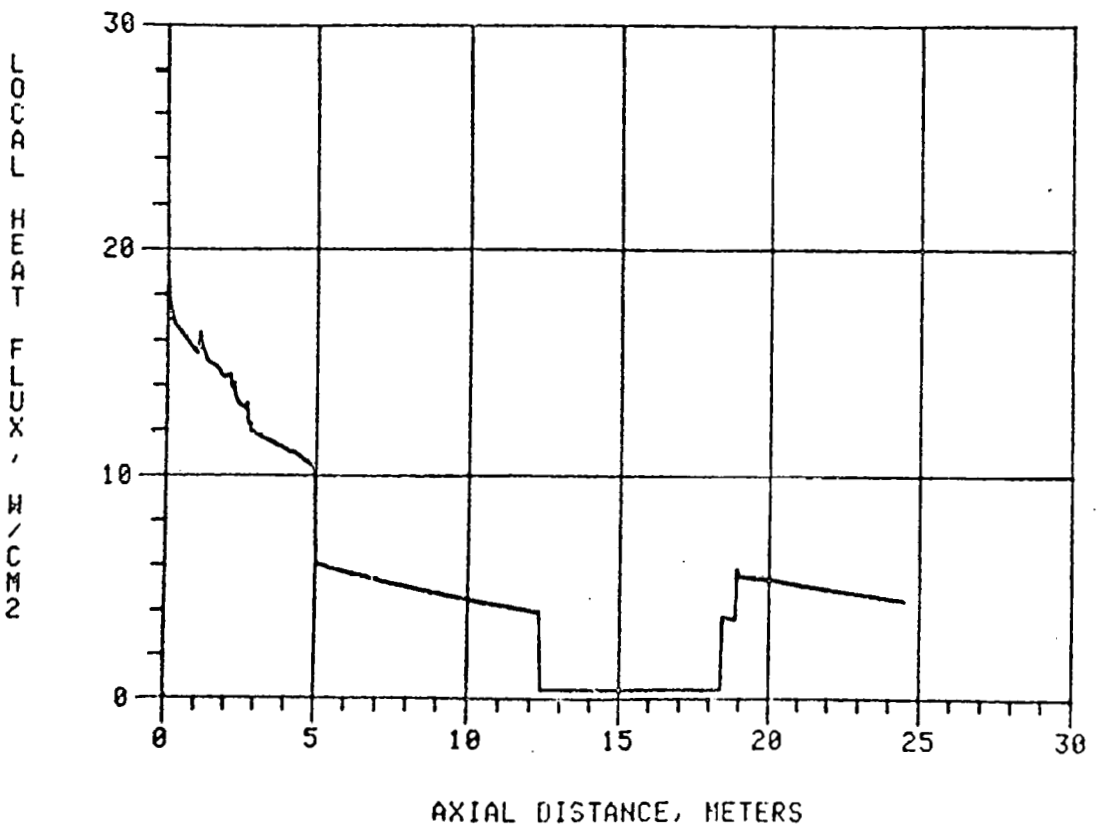

Figure 4.2b Local Heat Flux Distribution, Test LMF1C-5, Step 8

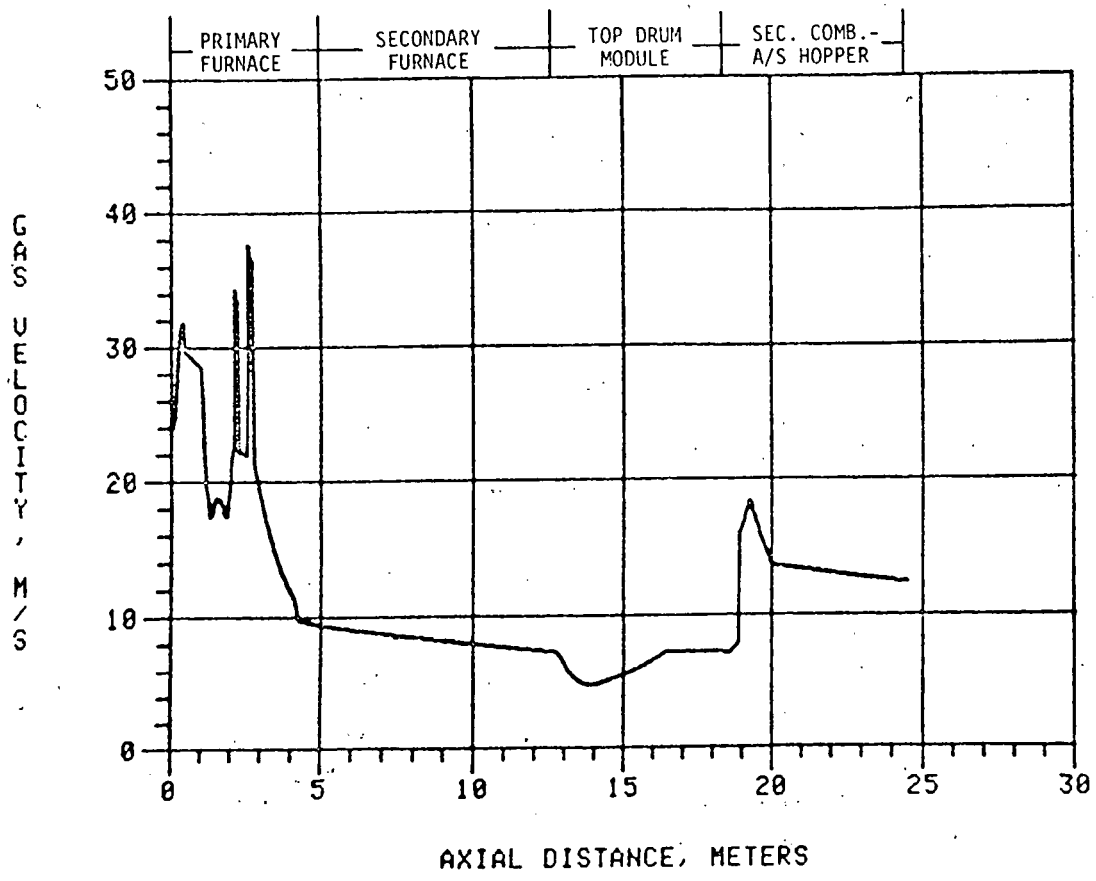

Figure 4.3a Gas Velocity Distribution, Test LMF1C-5, Step 8

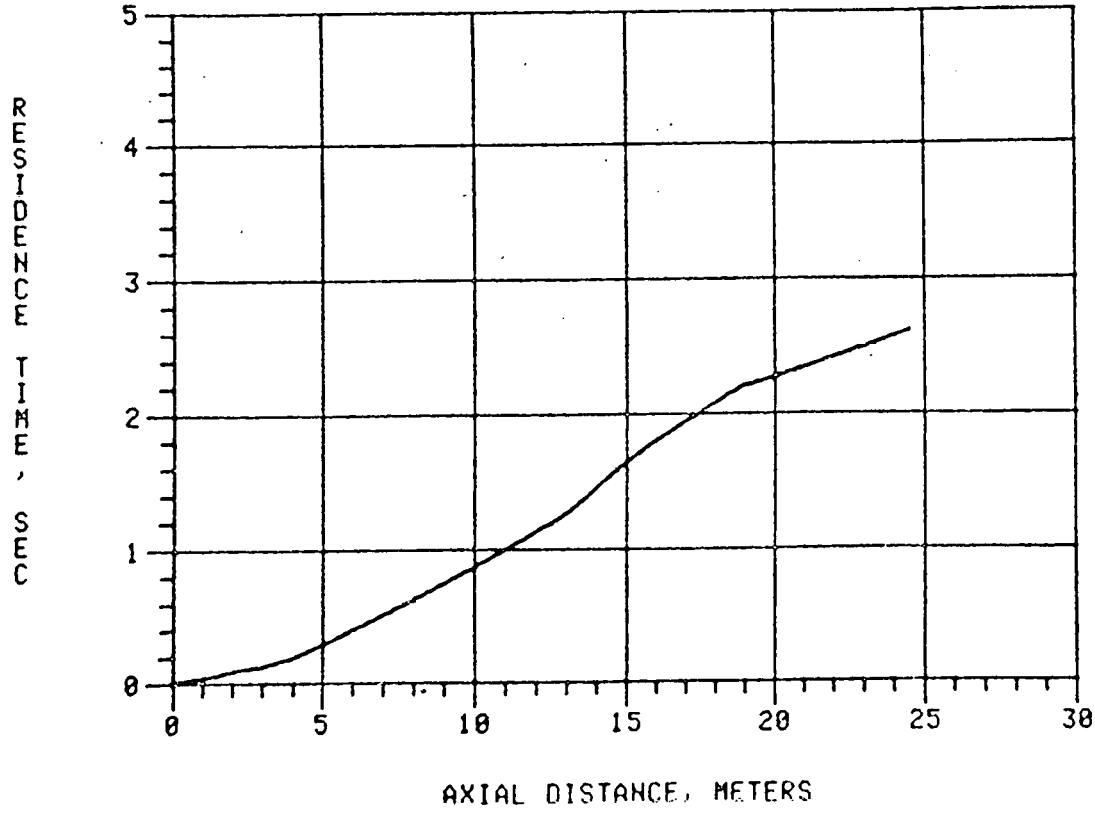

Figure 4.3b Gas Residence Time, Test LMF1C-5, Step 8

The total residence time calculated for this step is approximately 2.7 seconds. Residence time coupled with the temperature distribution are then used as inputs for NO_x relaxation calculations.

Figures 4.4a, b, c and d show temperature distributions for four steps in test LMF1C-3. Data comparison for these cases also appears to be good.

Finally, two predicted temperature distributions from test LMF1C-04 are presented in Figure 4.5. The purpose is to demonstrate the effect of primary N/O ratio on the level of the distribution. Step 8 has a slightly higher mass flow rate and an N/O ratio of 0.71, whereas Step 6 has an N/O ratio of unity. A "hotter" gas is produced at the lower N/O ratio and is reflected in the level of the distribution.

5.0 SUMMARY AND CONCLUSIONS

An overall review of the heat transfer code developed specifically for the DOE CFFF downstream components has been presented. The basic methods by which the gas state, transport properties, and the thermal radiative and convective properties are calculated have been delineated. Since the thermal behavior of the furnace is radiation dominated, a greater emphasis was placed on this mode of heat transfer.

The heat transfer model employs a single zone approximation to the physical problem. The results of the code show good agreement with the experimental data. A more rigorous approach to the problem requires the use of a multi-zone analysis which is presently under consideration.

The LMF1D tests (planned as the next series in the CFFF) are of long duration at a single fixed operating point. This will better enable experimental determination of the system heat loss for comparison to analysis. Heat flux probes will be placed in the system at various locations to extract information on local "point" conditions. In addition, more thermocouples will be installed downstream of the secondary combustor in order to verify the secondary combustion flame temperature calculation.

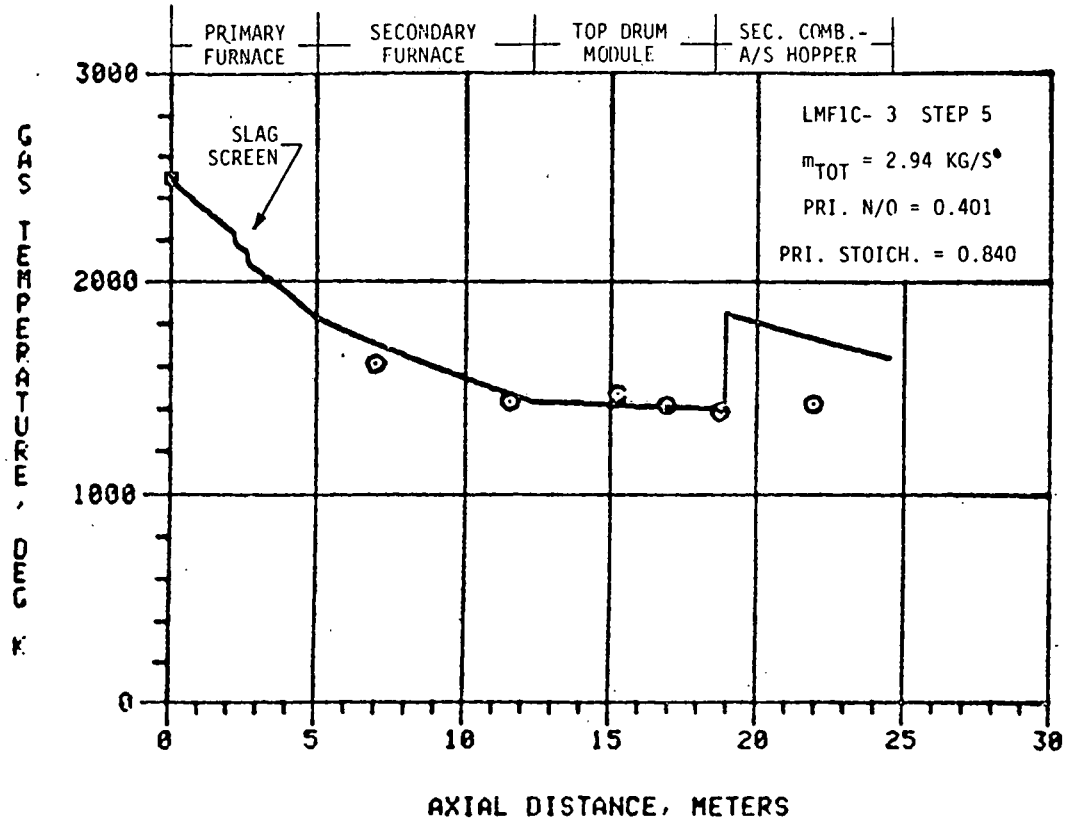

Figure 4.4a Gas Temperature Distribution, Test LMF1C-3, Step 5

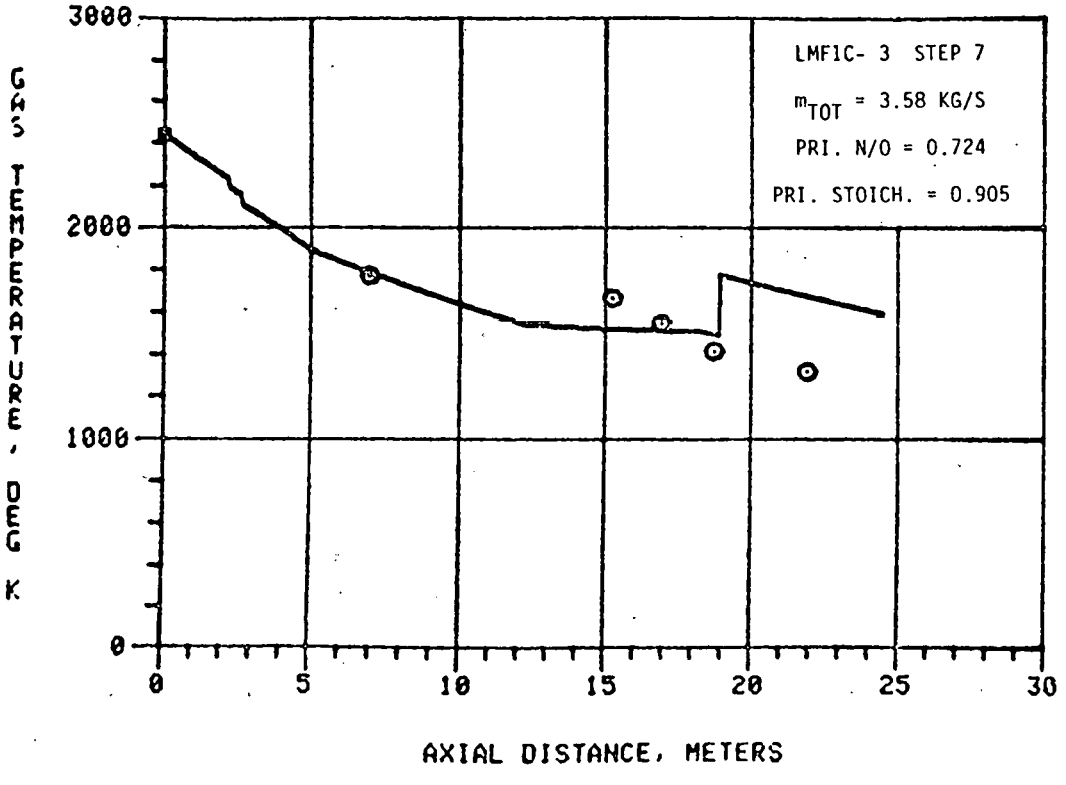

Figure 4.4b Gas Temperature Distribution, Test LMF1C-3, Step 7

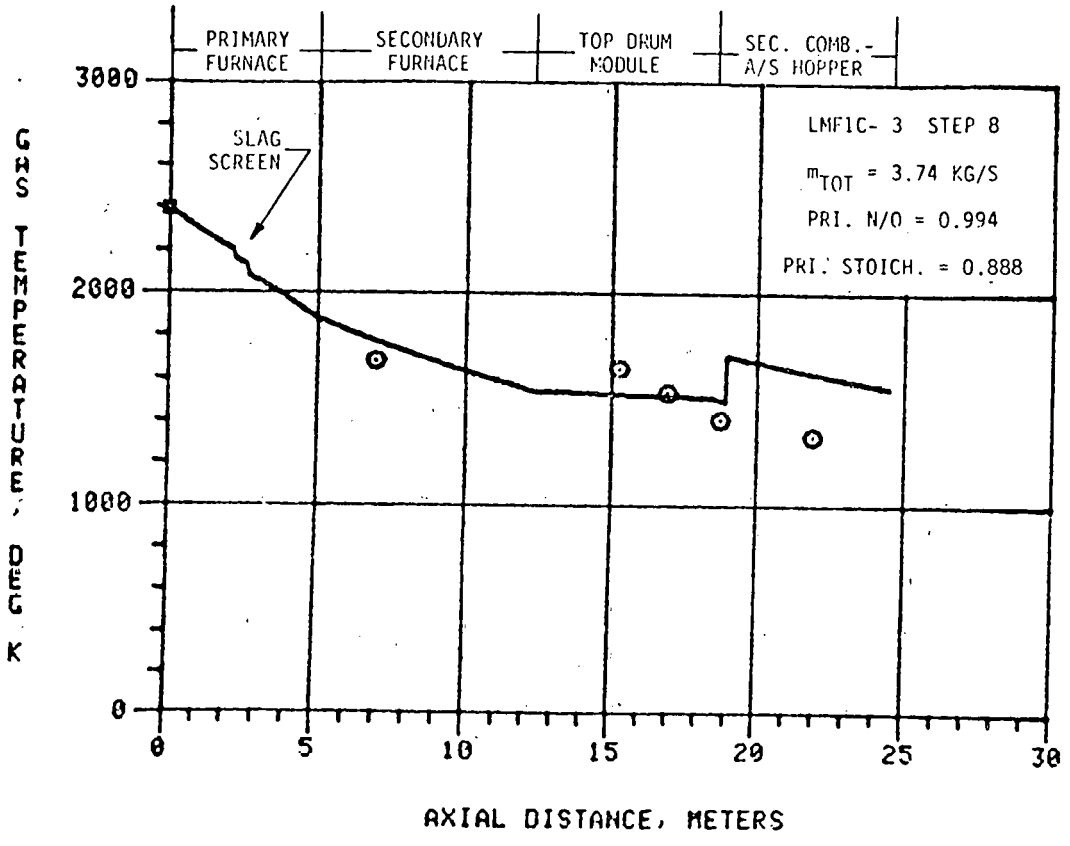

Figure 4.4c Gas Temperature Distribution, Test LMF1C-3, Step 8

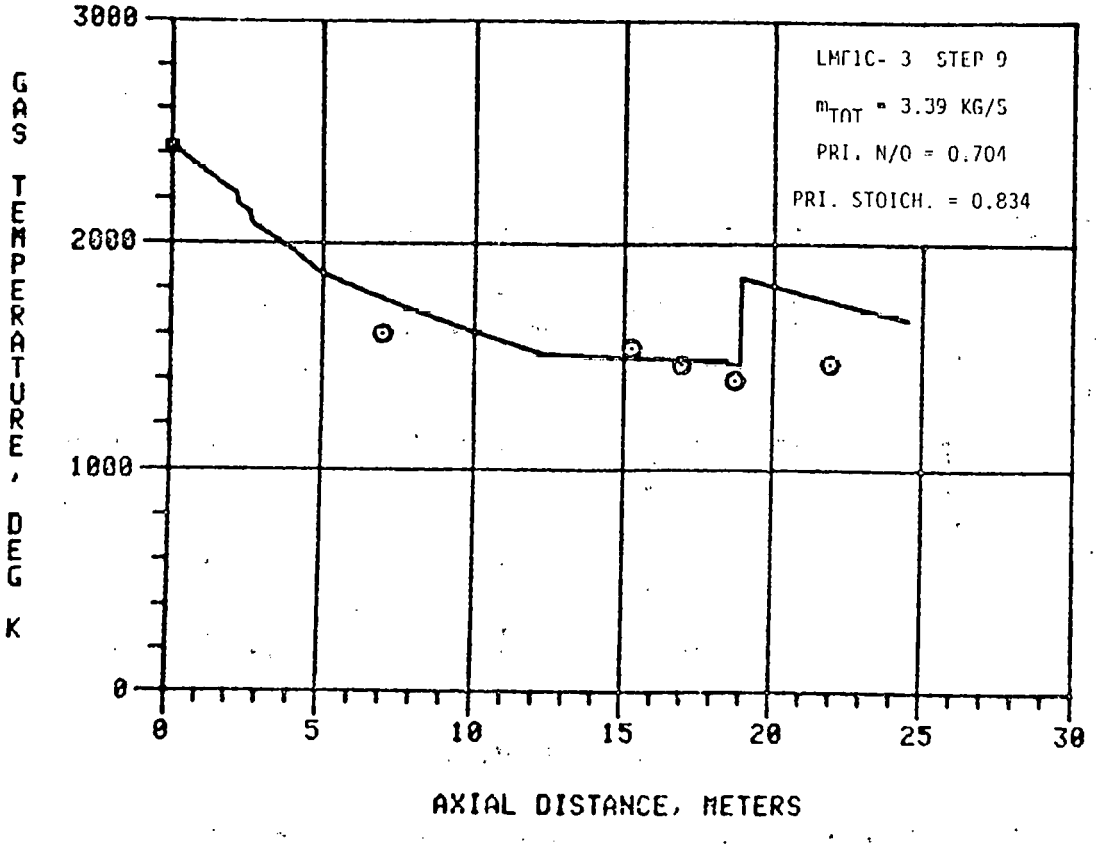

Figure 4.4d Gas Temperature Distribution, Test LMF1C-3, Step 9

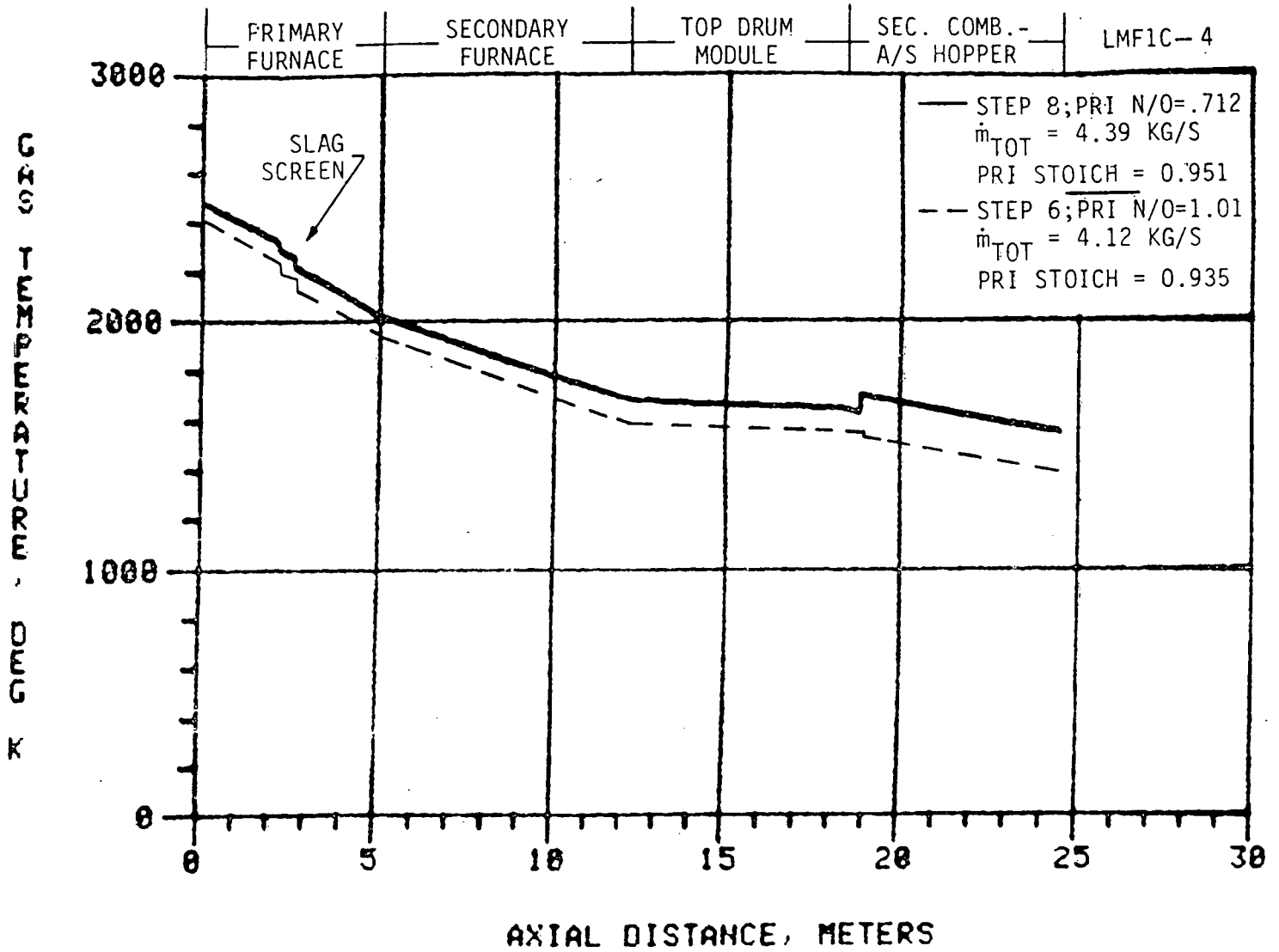

Figure 4.5 Gas Temperature Distributions, Test LMF1C-4, Steps 6 & 8

6.0 REFERENCES

1. Hottel, H. C.: in W. H. McAdams, Heat Transmission, 3rd ed., Chapter 4, McGraw-Hill, New York, 1954.

2. Ullrich, W., Sc. D. Thesis in Chemical Engineering, M.I.T., Cambridge, Massachusetts, 1936.

3. Ludwig, C. B., et al, "Handbook of Infrared Radiation from Combustion Gases, NASA SP-3080, 1973.

4. Hottel, H. C. and Sarofim, A. F., Radiative Transfer, Chapter 6, McGraw Hill, New York, 1967.

5. Hottel, H. C., and Manglesdorf, H. G., Transaction American Institute of Chemical Engineers, Vol. 31, p. 517, 1935.

6. Hottel, H. C. and Smith, V. C., Transaction ASME, Vol. 57, p. 463, 1935.

7. Egbert, R. B., Sc.D. Thesis in Chemical Engineering, M.I.T., Cambridge, Massachusetts, 1941.

8. Hottel, H. C. and Egbert, R. B., Trans. American Institute of Chemical Engineers, Vol. 38, pp. 531 - 565, 1942.

9. Foster, P. J. and Howard, C. R., "Optical Constant of Carbon and Coals in the Infared," Carbon, Vol. 6, p. 719, 1968.

10. Hottel, H. C. and Broughton, F. P., Industrial Engineering Chemistry, Analytical Edition, Vol. 4, p. 166, 1932.

11. Yuen, W. W. and Tien, C. L., "A Simple Calculation Scheme for the Luminous-Flame Emissivity," 16th International Symposium on Combustion, pp. 1481 - 1487, 1976.

12. Frederickse, H. P. R. and Hosler, W. R., "Electrical Conductivity of MHD Channel Material," 14th SEAM, The University of Tennessee Space Institute, April, 1974.

13. Siegel, R. and Howell, J. R., Thermal Radiation Heat Transfer, McGraw Hill, New York, 1972.

14. Siddall, R. G. and McGrath, I. A., "The Emissivity of Luminous Flames," 9th Symposium (International) Combustion, W. G. Berl, ed. pp. 102 - 110, 1963.

15. Sistino, A. J., "Analytical Studies of NO_x Decomposition in the Radiant Boiler of an Open-Cycle MHD Power Plant," ANL/MHD-79-7, Argonne National Laboratory, Argonne, IL, April 1979.

16. Sha, C. W., and Schulz, R. J., "Calculation of Thermodynamic, Transport, Electrical and Compositional Properties of Seeded Coal Combustion Plasma and its Effects on MHD Generator Performance," Internal Report, OR-10815-7, The University of Tennessee Space Institute, Tullahoma, TN, April 1982.

17. Anon, Program 25084 Combustion Gas Conductivity, Combustion of Coal, Kerosene, K_2CO_3 and Oxygen Enriched Air, Argonne National Laboratory.

18. Bunde, R., et al, MHD Power Generation, Springer-Verlag, Berlin, 1975.

19. Kreith, F., Principles of Heat Transfer, 3rd ed. Intext Educational Publishers, New York, 1973.

20. Eckert, E. R. G. and Drake, R. M., Analysis of Heat and Mass Transfer, McGraw-Hill, New York, pp. 403-412, 1972.

21. Galanga, F. L. and Lineberry, J. T., "Experimental and Theoretical Evaluation of the CFFF LMF Power Train," AIAA Paper No. 83-1746, to be presented at the AIAA 16th Fluid and Plasmadynamics Conference, Danvers, MA, July 11-14, 1983.

☆ U.S. GOVERNMENT PRINTING OFFICE 1984—746-081/2529